Boron isotope pH calibration of a larger benthic nummulitid foraminifer using LA-MC-ICPMS

Douglas Coenen[a,b*], *David Evans*[a,b,†], *Hagar Hauzer*[c,d], *Romi Nambiar*[a,b], *Hana Jurikova*[e], *Matthew Dumont*[e], *James Rae*[e], *Jonathan Erez*[c], *Laura Cotton*[f], *Willem Renema*[g.h], *Wolfgang Müller*[a,b]

[a] Institute of Geosciences, Goethe University Frankfurt, Frankfurt am Main, Germany

[b] Frankfurt Isotope and Element Research Center (FIERCE), Goethe University Frankfurt, Frankfurt am Main, Germany

[c] The Fredy and Nadine Hermann Institute of Earth Sciences, The Hebrew University of Jerusalem, Jerusalem, Israel

[d] Israel Oceanographic and Limnological Research, National Institute of Oceanography, Haifa, Israel

[e] School of Earth and Environmental Sciences, University of St Andrews, St Andrews, United Kingdom

[f] Natural History Museum of Denmark, Copenhagen, Denmark

[g] Naturalis Biodiversity Center, Leiden, Netherlands

[h] Institute of Biodiversity and Ecosystem Dynamics, University of Amsterdam, Netherlands

[*] Corresponding author: coenen@geo.uni-frankfurt.de

[†] Present address: School of Ocean and Earth Science, University of Southampton, Southampton, United Kingdom

Abstract

The boron isotope paleo-pH/CO_2 proxy is one of the key quantitative tools available to reconstruct past changes in atmospheric CO_2 concentration. Marine calcifiers have proven to be useful archives of this proxy to reconstruct variations in pH/CO_2 throughout the Cenozoic. In order to provide an alternative proxy carrier to the widely used planktonic foraminifera, we utilize ~~used~~ the symbiont-bearing, high-Mg, shallow-dwelling, tropical benthic species *Operculina ammonoides* (larger benthic foraminifera, LBF) and present a calibration of the relationship between pH and its boron isotopic composition, expressed as $\delta^{11}B$. We investigated specimens both live-collected from several reefs as well as from laboratory culture experiments in which pH and DIC were decoupled from each other. Our data were generated using laser-ablation as sample introduction technique. Based on laboratory culture samples, our resulting linear relationship between the *in-situ* boron isotopic composition of aqueous borate ion ($B(OH)_4^-$) and the shells of *O. ammonoides* gives a gradient of $0.38_{-0.10}^{+0.12}$. In contrast, the boron isotopic composition of the live-collected samples in the field displays a near 1:1 relationship with $B(OH)_4^-$. We suggest that this discrepancy, and the shallow slope of the laboratory culture regression, results from the difference between the carbonate chemistries in their respective micro-environments and surrounding seawater, driven by a pH dependence of the relative rates of calcification and photosynthesis. Based on a model of the effect of these processes on the diffusive boundary layer, we show that this effect is expected in laboratory culture experiments free from micro-turbulence, but not in the foraminifer's natural environment. As such, we demonstrate the utility of these organisms as proxy carrier, while also highlighting how laboratory experimental design has the potential to drive important changes in the micro-environment of organisms of this size. Given that the genus *Operculina* originated in the late Paleocene, this work paves the way towards deep-time paleo-pH/CO_2 reconstructions using larger foraminifera.

Keywords: Boron isotopes, LA-MC-ICPMS, foraminifera, pH proxy, laboratory calibration.

1. Introduction:

Understanding the climate of Earth's geological past is key in characterising the broad features of warm climate states (Poloczanska et al., 2018) and represents an important method of assessing state of the art model performance (Tierney et al., 2020). During the Cenozoic (66 Ma to present), the climate evolved from a hothouse, with global temperature ~15°C higher than pre-industrial during the early Eocene (Inglis et al., 2020), to an ice-house world, ultimately characterised by bipolar ice sheets in the past 3.3 Myrs (Zachos et al., 2001). This long-term change was punctuated by a number of climatic events, the study of which is key to understanding the complex relationship between climate, greenhouse gas concentrations, the biosphere and Earth's surface processes (e. g. Westerhold et al., 2020).

Accurate and precise reconstructions of past changes in CO_2 are a prerequisite for constraining climate sensitivity from paleo-data (e.g. Anagnostou et al., 2016), with direct relevance to better understanding the likely magnitude of future global warming (PALAEOSENS, 2012). Within the scope of these broad aims, a key quantitative methodology for reconstructing CO_2 beyond the ice-core records is based on the boron isotopic composition of marine biogenic calcite (Sanyal et al., 1995; Hönisch et al., 2009; Rae, 2018).

The boron isotope proxy is based upon the pH-dependent aqueous speciation of boron, with boric acid ($B(OH)_3$) and borate ion ($B(OH)_4^-$) dominating at low and high pH, respectively (Dickson, 1990). Being a light element, there is a large fractionation in the boron isotopic composition between these two species at low temperature, as they are characterised by a substantial difference in bond lengths between the B and OH group (Branson, 2018a). As a result, the boron isotopic compositions of both species changes in tandem with their proportions in solution, which in-turn is dominantly driven by pH, given that boric acid is weakly dissociative. If $B(OH)_4^-$ is the only, or dominant, species incorporated into $CaCO_3$, then the boron isotopic composition of the mineral should scale with the pH of the solution from which it was precipitated. In the case of marine calcifiers (especially foraminifera) it was initially hypothesised that only $B(OH)_4^-$ is incorporated into their calcite shell (Hemming and Hanson, 1992), as appears to be broadly the case for aragonite (Trotter et al., 2011; Anagnostou et al., 2012; McCulloch et al., 2017; Gagnon et al., 2021). However, many studies have since shown that there are significant kinetic and/or vital effects on boron incorporation into the shell of calcitic marine organisms (Zeebe et al., 2003; Hönisch et al., 2003; Foster, 2008; Rollion-Bard and Erez, 2010; Henehan et al., 2013, 2016).

For these reasons, the application of the proxy to the fossil record generally requires the development of empirical calibrations, which account for the "vital effects" resulting from the biological process of calcification or kinetic processes involved in mineral growth (Sanyal et al., 1996; Henehan et al., 2013).

Here, we focus on *Operculina ammonoides*, a high-Mg calcite larger benthic foraminifera (LBF) of the family Nummulitidae (Cotton et al., 2020). These foraminifera are symbiont bearing, shallow water tropical reef dwellers favouring oligotrophic conditions and a sandy substrate (Renema and Troelstra, 2001) that typically live at depths of 10 to 70 m (Hohenegger et al., 1999; Renema, 2002; Oron et al., 2018). The advantages of working with these LBF are that i) their large size facilitates multiple geochemical measurements on the same individual specimens (e.g. $\delta^{11}B$ and major/minor/trace elements) and ii) the nummulitid foraminifera have a lineage extending back to the late Paleocene, for example, the genus *Operculina* originated in the early Eocene (Hottinger, 1977). ~~Recent molecular work by Holzmann et al. (2022) suggested the reclassification of *O. ammonoides* to the new genus *Neoassilina*, however this is not currently in common use and if this is the case *Neoassilina* would also be closely related to Operculina both extinct and extant.~~. ~~It is worth noting that some species of *Operculina* and *Assilina*n from the fossil record are so similar that their affinity is not determined and genus *Operculina* and *Assilina* are used interchangeably or alongside one another (Hottinger, 1977; Özcan et al., 2019).~~ Previous work has demonstrated that Eocene and modern representatives of this group are characterised by a similar shell (trace) element composition (Evans et al., 2013), suggesting that the biomineralisation strategy and related vital effects between the modern and fossil representatives of this family are very similar. As such, the calibration presented here (see below) may be applicable to deep-time (Paleogene) samples with a degree of confidence that may be difficult to obtain in some other foraminifera groups.

Here, we analysed *Operculina ammonoides* grown in a laboratory culture experiment in which aspects of seawater carbonate chemistry were varied independently of each other, i.e. varying DIC at constant pH, and vice versa. Samples of the same species were also collected from a number of reefs in the Indo-Pacific to compare the boron isotopic composition of this species in its natural environment to that of the controlled laboratory setting.

We used laser ablation as an analytical technique coupled to a multi-collector inductively coupled plasma mass spectrometer (LA-MC-ICPMS) to generate a calibration of the relationship between the boron isotopic composition of foraminifera and seawater carbonate/boron chemistry. The relatively large test size of LBF (compared to planktonic or smaller benthic foraminifera) also makes these an ideal target for *in-situ* elemental and isotopic measurements (Evans et al., 2015; Van Dijk et al., 2017).

2. Materials and methods:

2.1 Laboratory culture experiments

Specimens of *Operculina ammonoides* were collected from the North Beach in the Gulf of Eilat, Israel in 2018. Bulk sediment containing abundant foraminifera was collected at a water depth of around 22 m, following which the bulk sample was transferred to the Institute of Earth Sciences at the Hebrew University of Jerusalem. Live foraminifera were identified as those that climbed on vertical glass slides. The live foraminifera were sieved to retain specimens with uniform size (HH6: 350-475 μm and HH7: 475-690 μm).

Before transfer to the experimental seawaters, the foraminifera were placed in jars filled with seawater from the Gulf of Eilat with 40 μM calcein for five days (Erez, 2003; Evans et al., 2015; Hauzer et al., 2018). This membrane impermeable fluorescent dye enables chambers precipitated during the experimental period to be identified, as those grown in the jars before transfer to experimental seawaters will incorporate the dye, while the chambers grown during the experiment will not (Figure 1a).

In addition, all culture seawaters were isotopically labelled with 74 nM ^{135}Ba (93%) to provide another means of unambiguously distinguishing newly precipitated chambers from those formed prior to collection (Evans et al., 2016). The low concentration of Ba in seawater (<10 μmol/mol) and the low natural abundance of ^{135}Ba (natural ^{135}Ba/^{138}Ba of 0.0919; Rosman and Taylor, 1997) enabled a small increase in the seawater [Ba^{2+}] to achieve an order of magnitude difference between the natural and experimental seawater ^{135}Ba/^{138}Ba; the culture seawater was characterised by a ^{135}Ba/^{138}Ba of ~1. Because each experiment was spiked individually, there were small differences in the seawater ^{135}Ba/^{138}Ba between the experiments (between 0.7 and 1.2, see Fig. S1). Once prepared, these seawater reservoirs were stored in airtight foil-lined inflatable bags to prevent re-equilibration of the carbonate system with the atmosphere.

The incubation of foraminifera was conducted in glass jars containing 120 mL of experimental seawater. The cultured foraminifera experienced a 12 hours dark-light cycles, with around 40 μM photons m^{-2} s^{-1}, with both natural and fluorescent light. The foraminifera were fed with 50 μL of frozen algae *Isochrysis* after each water exchange.

Two main sets of experiments (HH6 and HH7) were conducted in which the concentration of dissolved inorganic carbon (DIC) and pH were decoupled from each other (Hauzer, 2022). To investigate the control of pH on the incorporation of boron and boron isotopes in *O. ammonoides*, in the first of these experiment sets (HH6) pH was varied at near constant DIC from ~7.4 to ~8.4 (Table 1) by changing the alkalinity of natural Gulf of Eilat seawater via HCl or NaOH addition (DIC = 2200 ± 119 µmol/kg$_{sw}$, 2SD variation between the experimental means). Salinity was unmodified at 40.65. In addition, two experiments were conducted at an elevated Ca^{2+} concentration ([Ca^{2+}_{sw}]; 13.7 and 17.7 mmol/mol respectively) and lower than natural pH, to explore the potential influence of past changes in [Ca^{2+}_{sw}] on *O. ammonoides* $\delta^{11}B$. Around 50 individuals of *O. ammonoides* were used per experiment. In contrast, the experiment set HH7 was designed to evaluate the possible control of seawater DIC on boron incorporation in *O. ammonoides* by keeping the pH constant (pH_{NBS} = 7.90 ± 0.28, 2SD variation between the experimental means) and varying DIC concentration between 825 and 2460 µmol/kg$_{sw}$. The seawater used for HH7 was adjusted to a salinity of 37 by diluting seawater from the Gulf of Eilat with deionised water. For this set of experiments, around 80 individuals of *O. ammonoides* were used for each experiment.

The water of the experimental jars was exchanged every ten days with seawater from the reservoirs. Before the exchange, the pH and alkalinity of both the culture jars and reservoirs were measured and were used to calculate the population growth rates of the foraminifera via alkalinity depletion (Segev and Erez, 2006; Oron et al., 2020) as well as to calculate the rest of the carbonate system (i.e. DIC, HCO_3^-, CO_3^{2-} and Ω_c) using the Python version of CO2SYS (Lewis and Wallace, 1998; Humphreys et al., 2020). Details of the constants used to do so as well as error propagation are given in section 2.4. The culture jars were kept at a constant temperature of 25°C (±0.2°C) by placing them into a water bath controlled by simultaneous cooling and heating (e.g. Evans et al., 2015). After 60 days, the experiment ended by washing the foraminifera with deionised water, after which they were dried and stored for later analysis. Before geochemical analysis, the samples were treated overnight with NaOCl to remove organic material and rinsed several times with deionised water. Finally, a further series of ethanol and Milli-Q (18.2 MΩ) cleaning steps, one and two steps respectively including 30s ultrasonication were performed a few days before laser ablation analysis at the Frankfurt Isotope and Element Research Center (FIERCE) laboratories to remove any residual surface contaminants.

2.2 Laboratory culture carbonate chemistry calculations

While every attempt was made to maintain constant carbonate chemistry conditions in both the culture jars and seawater reservoirs (Hauzer, 2022), some drift occurred in both cases as a result of calcification/photosynthesis/respiration of the foraminifera, and as a result of a small amount of leakage or possible bacterial growth in the reservoirs. As such, the pH and DIC drifted by an average of 0.37 and 206 µmol/kg_{sw} respectively over the course of the experiment in the culture jars (see Table 1 and Fig. S2a). Three different methodologies were used to explore the sensitivity of our results to this variation/drift:

1. Simple means of all carbonate system measurements from the culture jars were calculated. This assumes that any drift in the seawater reservoirs must be included in the culture jar measurements.
2. Averages of the average between the pairs of culture jar and seawater reservoir measurements were calculated. This accounts for the fact that the foraminifera modify the carbonate chemistry of the seawater in the culture jars, e.g. via calcification. As such, the average conditions experienced by the foraminifera may be best reflected by the midpoint of the measurements in the jars and reservoirs.
3. Bulk population growth rate curves were calculated using the alkalinity depletion method (e.g. Hauzer et al., 2018), following which these curves were used to generate weighted averages of pH and DIC. This weights the reported measurements towards the portions of the experiment in which the overall growth rate was highest. This method was applied to both the culture jar measurements (method 1 above) and the average of the paired culture jar and seawater reservoir measurements (method 2).

It is not immediately clear which of the above methods is most appropriate when interpreting geochemical data. Previous work has demonstrated that, when culturing LBF, the resulting individual specimen calcification rates may vary greatly within the population (Hauzer et al., 2021). Some may live longer than others or some may calcify mainly at the beginning of the experiment, others may continue to calcify at a broadly constant rate irrespective of changes in the bulk population growth rate measured by alkalinity depletion. The question becomes: given a drift in pH/DIC with time, are the analysed chambers more likely to come from the part of the experiment when the overall population growth rate was higher? If so, a growth-rate weighted average might be appropriate. Since we selected specimens with at least one chamber precipitated in culture on the basis of calcein labelling, we consider it likely that we analysed foraminifera that stopped calcifying part-way through the experiment, such that average values of the seawater carbonate chemistry weighted to the population growth rates are likely to be the most appropriate characterisation of the conditions that the foraminifera experienced.

Specifically, we derived weights through time using the proportion of total growth that had taken place at the point of each water exchange and used this as a weight to calculate weighted average and weighted standard error (following Gatz and Smith, 1995) of pH and total alkalinity (see Table 1). However, we note that none of our main conclusions are sensitive to this data treatment and all possible alternative averages of measured pH and total alkalinity used for the experiment are also explored in the supplementary materials.

2.3 Field-collected samples

As paleoenvironmental reconstructions always use natural samples, we additionally included samples not grown in culture to constrain the natural variability of the proxy outside of the controlled environment (McClelland et al., 2021). Here, we analysed *Operculina ammonoides* samples collected from six different reefs in the Indo-Pacific, specifically the northernmost Red Sea, the Great Barrier Reef and three locations in Indonesia (see Evans et al., 2013; Renema, 2002, and references therein). The physical properties and chemical composition of surrounding seawater were not measured at the time of collection (Renema, 2002; Renema et al., 2013), therefore global ocean datasets were used instead, detailed below. Given that not all foraminifera were alive at the moment of collection, an average of the carbonate system parameters needs to be derived in order to encapsulate natural variability.

The updated dataset from Gregor and Gruber (2021) was used for pH and alkalinity with temperature data taken from OISSTv2.1, and salinity data from SODAv3.4.2. The reported values (Table 3) are the mean and 2SD of the dataset between 1990 and 2002 (144 months). The sample SSO7G14 from the Great Barrier Reef was collected live in 2012 (Renema et al., 2013) so a yearly average between 2010 and 2012 was taken instead. Gregor and Gruber (2021) note that the scarcity of reliable data before 1990 means that older results should be interpreted with care, so we decided to only sample data from 1990 to 2002, which in any case almost certainly encompasses the interval in which these foraminifera lived. We note that some regions of interest (especially Indonesia) have only a few measurements in the desired time interval and rely mainly on the trained machine learning algorithms of Gregor and Gruber (2021) to fill the gaps. Seawater pH was measured near islands in the Spermonde Archipelago near Makassar (Sulawesi, Indonesia) in close proximity to the sample sites of KKE30 and BBX49a, the values of which differ by ~0.20 and ~0.16, respectively, from the datasets of Gregor and Gruber (2021), resulting in a difference in calculated $\delta^{11}B_{B(OH)4-}$ of 2.02 and 1.63 ‰ respectively. The implications of this discrepancy will be further discussed in section 4.1.

Although temperature has a relatively minor effect on $\delta^{11}B_{B(OH)4-}$ compared to pH (Foster and Rae, 2016; Zeebe and Wolf-Gladrow, 2001), it is important for the accuracy of the reconstruction. Similarly to pH, the temperature dataset of OISST is designed for the open ocean as it is based on a combination of satellite, ship and buoy data (Huang et al., 2021). That is why we opted for previously reported mean annual temperature instead wherever possible (Evans et al., 2013).

2.4 Carbon and boron system calculations

The carbonate system was determined from measured pH_{NBS} and total alkalinity using CO2SYS for the carbonate system calculations, including the concentration of calcium where this was experimentally modified (see below), silicate (0.3 $\mu mol/kg_{sw}$) and phosphate (0.05 $\mu mol/kg_{sw}$). The equilibrium constants K_1 and K_2 were taken from Lueker et al. (2000). These are recommended by Dickson et al. (2007) and in addition, Raimondi et al. (2019) demonstrated the best internal consistency when reconstructing DIC from pH and total alkalinity when these constants are used.

Uncertainty was propagated via a Monte Carlo approach calling CO2SYS 10^5 times with random pH and total alkalinity values sampled from their uncertainty bounds (similar to Williams et al., 2017 and Raimondi et al., 2019), assuming a normal distribution in both cases. The non-linear relationship between pH and other constituents of the carbon system, when pH is the dominant uncertainty source in a sample, the resulting Monte Carlo dataset are not normally distributed (Lauvset and Gruber, 2014; Orr et al., 2018). Each simulated parameter was individually screened by testing their normality with D'Agostino's K-squared test (D'Agostino and Pearson, 1973 - used with Python implementation in SciPy - Virtanen et al., 2020). Example of parameter screening can be found in the supplementary materials (Figure S4). In the case of a normally distributed parameter, the median and 2SD are reported, otherwise, the median, 2.5th and 97.5th percentiles are reported (Tables 1-3).

The values of pK_b^* and $\delta^{11}B_{B(OH)4-}$ were calculated using the Python package *cbsyst* (Branson, 2018b) containing a fast implementation of MyAMI, which incorporates the pairing effects of Ca and Mg on different equilibrium constants (Hain et al., 2015, 2018), and carbon/boron system simulation following CO2SYS. The use of MyAMI was especially relevant for the experiments HH6-5 and HH6-6 (Table 1) as they were both characterised by a higher Ca^{2+} concentration than natural seawater, which changed K_B^* by ~1 and 3% respectively. We used a boron species fractionation factor (α_B) value of 1.027 ± 0.0006 (Klochko et al., 2006). The value used for the $\delta^{11}B$ of seawater was 39.61 ± 0.04 ‰ (Foster et al., 2010). Similarly to other carbon system parameters, 10^5 Monte Carlo simulations of the boron system were generated from pH data as well as temperature, salinity, $\delta^{11}B_{sw}$ and α_B.

To explore whether speciation controls the incorporation of boron in *Operculina ammonoides*, we used the PHREEQC model (Parkhurst and Appelo, 2013) to calculate the concentration of $CaB(OH)_4^+$ and $MgB(OH)_4^+$ ion pairs in the experimental and natural seawaters, as well as activity coefficients of the carbonate and boron species. We used the PITZER database which is more suitable for application to solutions with higher ionic strength like seawater (I ~0.7) (Farmer et al., 2019; Henehan et al., 2021; Nir et al., 2015). We followed the recommendations of Nir et al. (2015) and applied an offset of 0.19 to the pH total scale to compensate the Macinnes assumption used in PHREEQC, so the culture pH_{NBS} measurements were first converted to the total scale using CO2SYS to then apply the offset. The ionic composition of seawater was scaled with salinity (following Millero, 2005; and following Lee et al., 2010 for boron) except for calcium (which was taken from culture solution measurement). For the uncertainty of the simulations, a Monte Carlo approach was used by performing 10^4 simulations with randomly sampled pH_{tot}, alkalinity, temperature and salinity. The reported values are the median and $2.5^{th}/97.5^{th}$ percentiles. Similarly to Farmer et al. (2019), we observe an offset between pK_b^* calculated using PHREEQC and CO2SYS/*cbsyst*, ranging from 0.088 to 0.093.

2.5 Boron isotope and B/Ca analytical details

All boron isotopic measurements were performed using the LA-MC-ICPMS setup at the Frankfurt Isotope and Element Research Center (FIERCE) at Goethe University Frankfurt, following the methodology outlined in Evans et al. (2021). In brief, a RESOlution LR 193nm ArF laser ablation system (Applied Spectra, formerly Resonetics (Müller et al., 2009)) was connected to a Neptune Plus MC-ICPMS (Thermo-Fisher Scientific). The RESOlution LR is equipped with the two-volume Laurin Technic S-155 laser ablation cell. It was used with Helium as the main cell gas, with the Ar sample gas from the MC-ICPMS admixed into the top of the inner cell funnel. N_2 was added downstream of the ablation cell to improve sensitivity (Lin et al., 2014). Nylon-6 tubing was used throughout as it ensures lower-B background (Evans and Müller, 2018).

To distinguish between the chambers grown in the controlled environment (in ^{135}Ba-enriched seawater (Evans et al., 2016)) from those which did not, the $^{135}Ba/^{138}Ba$ of the foraminifera marginal cord was measured alongside the boron isotopic measurements. Ideally, the barium isotopic ratio would have been measured on the same spot as the boron isotopic measurement. However, this could not have been done without peak hopping and concomitant loss of depth resolution of the measurement. Instead, $^{135}Ba/^{138}Ba$ measurements were made separately and immediately adjacent to the $\delta^{11}B$ measurements (see below).

For the boron isotopic measurements, the Faraday cups were arranged to simultaneously measure ^{10}B (L3) and ^{11}B (H4) as well as to monitor the Ca interference that is present across the mass range 10-11 on the Neptune (Sadekov et al., 2019; Standish et al., 2019; Evans et al., 2021). Specifically, we measured the elevated baseline that results from the ablation of Ca-rich materials at m/z 10.035 (L2, cf. 10.089 in Evans et al., 2021) and 9.979 (L4), although we ultimately only use the former in correcting the measurements. All the measurements were done at low mass resolution, with 10^{13} Ω resistors installed on all four cups.

All gas flows and mass spectrometer parameters were optimised daily. Tuning was carried out by ablating NIST SRM612 with a 90 µm spot at 6 Hz repetition rate and ~6 J/cm^2 fluence to achieve a sensitivity between 3-4 V.g/mg and a background measurement on ^{11}B between 0.5 to 1 mV.

Instrumental mass bias was corrected using sample-standard bracketing with NIST SRM612 as a primary standard. The matrix interference present on ^{10}B when ablating samples with a Ca matrix on the Neptune plus was empirically corrected by analysing three well characterised carbonate standards and using the relationship between their $\delta^{11}B$ inaccuracy (difference between measured $\delta^{11}B$ and accepted $\delta^{11}B$ value) and ^{11}B/10.035 (proportional to B/Ca) for all samples (Standish et al., 2019; Evans et al., 2021). The three pressed powder pellet carbonate reference materials used here were: JCt-1 (*Tridacna gigas*) and JCp-1 (*Porites sp.*), both prepared by Dr Edmund Hathorne (GEOMAR) with $\delta^{11}B$ equal to 16.39 ± 0.60 ‰ and 24.36 ± 0.45 ‰ respectively (2SD of interlaboratory means (Gutjahr et al., 2020), and MACS-3 (USGS synthetic calcite) with a $\delta^{11}B$ value of -0.57 ± 0.11 ‰ (2SD of three solution measurements, Standish et al., 2019). The secondary standards were randomly distributed throughout the analysis sequence, analysed in an identical way to the samples, with at least 15 of each within a typical 12-hour session. All boron isotope analysis were carried out with a ~1.049 s integration time for 40 s drilling/spot analysis, with all samples and standard measurements bracketed by 20 s of gas blank analysis.

Given the fragility of the cultured *Operculina ammonoides* samples, specimens were mounted vertically to ablate the marginal cord (Fig 1a) by carefully placing them onto a pressure sensitive adhesive. The marginal cord of the cultured samples was thin (<50 µm), so a 40x40 µm square spot size was the largest that could be used.

Following the data processing procedure described above and in detail in Evans et al. (2021), each analysis was individually screened to discard erroneous measurements or those in which the marginal cord was almost immediately broken, using the ^{11}B voltage and raw $^{11}B/^{10}B$, as well as images from the laser ablation camera system collected during analysis.

Reproducibility and accuracy were assessed using three secondary standards: the UWC-1 and UWC-3 marble standards, initially developed for SIMS oxygen isotope analysis (Edwards and Valley, 1998; Graham and Wada, 1998) and an in-house calcite standard (DE-B) which is an inorganic blue calcite acquired from a mineral dealership. UWC-1 has three reported solution-based measurement of $\delta^{11}B$ (7.77 ± 0.89 ‰, compiled in Standish et al., 2019). However, to our knowledge, no solution-based measurement was available for UWC-3 and DE-B. To address this, the boron isotopic composition of these two materials was determined via solution MC-ICPMS analysis in the St Andrews Isotope Geochemistry laboratories (STAiG) of the University of St Andrews, UK. Several grains of DE-B, separated from two different hand-crushed samples (DE-B1 and DE-B2), and two grains of UWC-3 were selected and powdered to give approximately ~1-2 mg aliquots for boron isotope analysis. Unlike laser ablation analysis, it is common practice to perform chemical pre-cleaning of samples prior to solution analysis. The possible impact of this pre-cleaning on $\delta^{11}B$ was tested by further splitting each sample into halves and performing the pre-cleaning step on one of them. The first half of each aliquot went through a full cleaning procedure designed for biogenic carbonates from sediments involving clay removal rinses with boron-free Milli-Q (18.2 MΩ) and an oxidative cleaning step using 1% H_2O_2 buffered with 0.1 M NH_4OH at 80 °C, before dissolution in 0.5 M HNO_3 (e.g. Barker et al. (2003); Jurikova et al. (2019)). The second half was rinsed twice with boron-free ultra-pure water (Milli-Q, 18.2 MΩ) and dissolved with the aid of ultrasonication in 0.5 M HNO_3.

Prior to boron isotope analyses, boron was purified from the $CaCO_3$ matrix using boron-specific anion exchange resin, Amberlite IRA 743, crushed and sieved to 63–106 µm. Dissolved blue calcite and UWC-3 aliquots were processed alongside RM NIST 8301 Foram (Stewart et al., 2021) and total procedural blanks (TPBs). Purified boron solutions were spiked with HF to aid boron wash out and measured in a 0.5 M HNO_3 + 0.3 M HF matrix (Zeebe and Rae, 2020) on a Thermo Scientific Neptune Plus MC-ICPMS equipped with a HF-resistant sample introduction kit and 10^{13} Ω resistors. Instrumental mass bias was corrected by standard sample-bracketing with a 10 ppb NIST SRM 951 solution. The average $\delta^{11}B$ for RM NIST 8301 Foram was 14.61 ± 0.19 ‰ (2SD, n = 4) and the TPBs were <7 pg B, negligible against the typical sample size of ~ 5 ng B.

No significant difference between uncleaned and cleaned values were observed giving the average $\delta^{11}B$ of -0.18 ± 0.32 ‰ (2SD, n = 10) for DE-B1, 0.14 ± 0.19 ‰ (2SD, n = 10) for DE-B2, so an average value of -0.02 ± 0.41 ‰ was used for the DE-B calcite in-house standard. UWC-3 yielded a value of 20.25 ± 0.08 ‰ (2SD, n = 2).

When comparing the intermediate precision of measured $\delta^{11}B$ from the three external calcite standards (UWC-1, UWC-3, DE-B) from 41 laser ablation sessions (days) with solution-MC-ICPMS measurements, we observe a near 1:1 relationship, with an average overall difference of ~ 0.89 ± 0.38‰ (2SD). The individual intermediate precision difference between laser ablation and solution derived values are as follow: UWC-1: 0.86 ± 0.31 ‰ (2SE), UWC-3: 0.72 ± 0.27 ‰ and DE-B: 1.09 ± 0.16 ‰ (Fig. S5).

The $^{135}Ba/^{138}Ba$ composition of the cultured foraminifera was measured close to the ablation pits of the $\delta^{11}B$ measurements. The Faraday cups were arranged to simultaneously measure ^{135}Ba (L2) and ^{138}Ba (H2). The large difference in $^{135}Ba/^{138}Ba$ (~10 times higher) between culture and non-culture material allowed for a smaller spot size of 15x15 µm and shorter analysis (5 s). The same repetition rate (6 Hz) and fluence (6 J/cm^2) as for the $\delta^{11}B$ measurements were used. The resulting $^{135}Ba/^{138}Ba$ were then associated with the closest boron isotope ablation to distinguish calcite precipitated during culture from that precipitated in the wild.

To determine whether B/Ca can be accurately characterised using the ^{11}B/10.035 ratio obtained during the isotopic analysis, trace element analysis for B/Ca measurements was performed on the same samples using a Thermo-Scientific ELEMENT XR SF-ICPMS at FIERCE, connected to the same laser ablation system (see Table S2). Tuning was performed daily by ablating NIST SRM612 at 6 Hz and 60 µm spot size to achieve a sensitivity of >6x10^6 cps of ^{238}U, ThO^+/Th^+ < 1%, Th/U?????? and m/z 44/22 < 2% (to monitor doubly-charged ion production). The marginal cord of the samples was ablated using a 50 µm spot at 3 Hz repetition rate, with the “squid” signal smoothing device added downstream of the ablation cell to obtain a stable signal (Müller et al., 2009). B/Ca ratios were determined using ^{43}Ca as an internal standard (Heinrich et al., 2003) and NIST SRM610 as an external standard using the value of Jochum et al. (2011). Data reduction was done using an in-house Matlab script (Evans and Müller, 2018). Accuracy of three secondary standards, namely GOR-128G, JCt-1 and MACS-3 (Jochum et al., 2005, 2019; Hathorne et al., 2013) was measured for each session. Typical accuracies for these secondary standards are ~4%, ~3% and ~2% respectively.

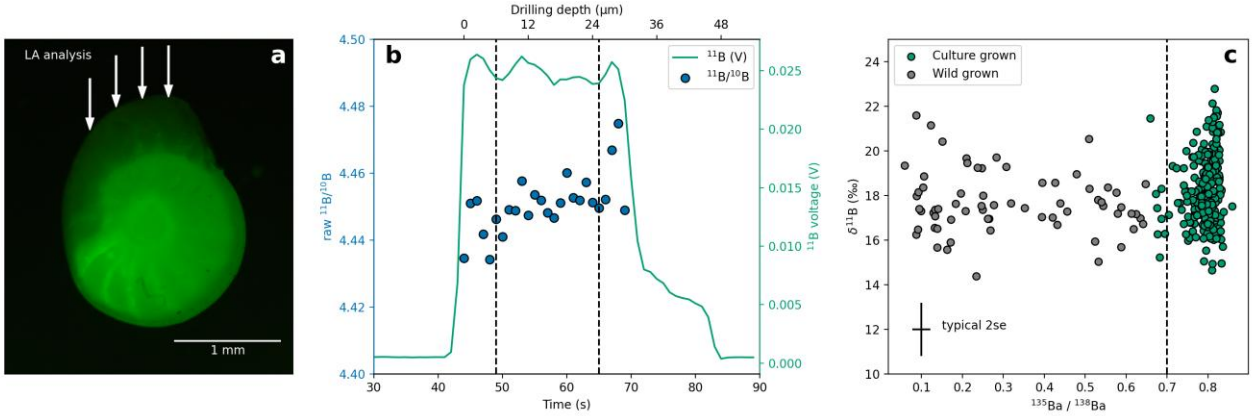

Figure 1: Example boron and barium isotope analysis of cultured Operculina ammonoides using LA-MC-ICPMS. (a) Fluorescent microscope picture of a cultured O. ammonoides illustrating the use of calcein to identify chambers precipitated in the laboratory. The low fluorescence chambers (top) are those grown during the culture experiment. The direction of the laser ablation analysis are depicted by arrows. (b) Example of a time resolved laser ablation analysis. The dashed vertical black lines depict the locations at which the data was trimmed in the case of this specific sample. The drilling depth was estimated using an ablation rate of 200nm/pulse at 6 J.cm^{-2}. (c) Example of using $^{135}Ba/^{138}Ba$ to unambiguously identify material grown in laboratory culture, plotted against $\delta^{11}B$ at a similar location in the shell (the Ba isotopic analyses were laterally offset by ~20 µm from the boron isotope analyses). The vertical dashed line represents the cut-off point representing a value 10% lower than the culture $^{135}Ba/^{138}Ba$ end member. The green data points are those that are within uncertainty of the cut-off points, considered to have come from material grown in controlled environment.

3. Results:

3.1 Boron isotope calibration

All results are displayed in Figures xx-yy and Tables x-y. The measured boron isotopic composition of the cultured *Operculina ammonoides* ranges between 16.09 ‰ (HH6-1, lowest pH experiment) and 19.45‰ (HH6-4, highest pH experiment) (Table 2). Most of the samples have a boron isotopic value heavier than the boron isotopic composition of *in-situ* aqueous $B(OH)_4^-$, with a greater offset at lower pH. The resulting boron isotope calibration of the cultured samples is plotted in Fig. 2 as a regression between measured $\delta^{11}B_{CaCO3}$ and calculated $\delta^{11}B_{B(OH)4-}$, based on physical and chemical properties of the water in which the foraminifera grew (Section 2.4; Henehan et al., 2013). Once a relationship between measured $\delta^{11}B_{CaCO3}$ and calculated *in-situ* $\delta^{11}B_{B(OH)4-}$ is derived, it allows for the conversion of future measurements into estimates of *in-situ* $\delta^{11}B_{B(OH)4-}$ which in turn can be used to estimate the *in-situ* pH.

As a result of non-linearities in the carbonate system (Section 2.4), the calculated $\delta^{11}B_{B(OH)4-}$ values are not normally distributed. Given that, to our knowledge, no linear regression algorithm available is able to take this kind of uncertainty into account, we determine the best-fit linear regression through the data using a Monte Carlo approach by performing linear regressions through 10^5 randomly generated $\delta^{11}B_{CaCO3}$ (within their uncertainty bounds) and $\delta^{11}B_{B(OH)4-}$, the latter derived as reported above. Since the uncertainties in $\delta^{11}B_{B(OH)4-}$ are not normally distributed, neither are the resulting gradients and intercepts and the resulting values are thus the median and the lower and upper bounds are the 2.5th and 97.5th percentiles (eq. 1).

$$\delta^{11}B_{B(OH)_4^-} = \frac{\delta^{11}B_{CaCO_3} - \left(11.71^{+1.47}_{-1.88}\right)}{0.38^{+0.12}_{-0.10}} \qquad \text{(Eq. 1)}$$

Based on a simple least-square regression, the goodness of fit statistics are as follows: R^2 = 0.83, Root Mean Square Error (RMSE) is 0.34 ‰ and p = 0.0001. With a gradient lower than one (0.38) in borate space, the boron isotopic calibration of cultured *O. ammonoides* appears to be less pH sensitive than $B(OH)_4^-$. The DIC concentration in the growth media does not appear to have a significant influence on the $\delta^{11}B$ composition of cultured *O. ammonoides*, a simple ordinary least squares (OLS) regression between DIC and $\delta^{11}B$ yields the following statistics: R^2 = 0.04, RMSE = 0.74 ‰, p = 0.52 (Fig. 2c). The weighted pH of experimental jars appears to be more significant than DIC to explain the trend in $\delta^{11}B_{CaCO3}$ (Fig. 2b). A non-linear logistic fit yields the following statistics: R^2 = 0.75 and RMSE = 0.38 ‰.

The wild specimens are characterised by measured $\delta^{11}B_{CaCO3}$ values ranging between 15.46 ‰ to 18.86 ‰ (Fig. 2, pink triangles) and their associated calculated *in-situ* $\delta^{11}B_{B(OH)4-}$ range from 16.25 ‰ to 19.08 ‰. These samples have a notably different, steeper trend of boron isotopic composition compared to the cultured specimens, and most seem to lie within uncertainty of the borate line (5 of 6 datapoints used). There are notable exceptions to this, especially the lowest $\delta^{11}B_{CaCO3}$ sample (SER, Table 2), which has a very different $\delta^{11}B_{B(OH)4-}$ value. It is considered as an outlier with a Cooks distance of 0.64. Otherwise, a forced linear fit with a gradient of 1 appears to be within uncertainty of the borate line.

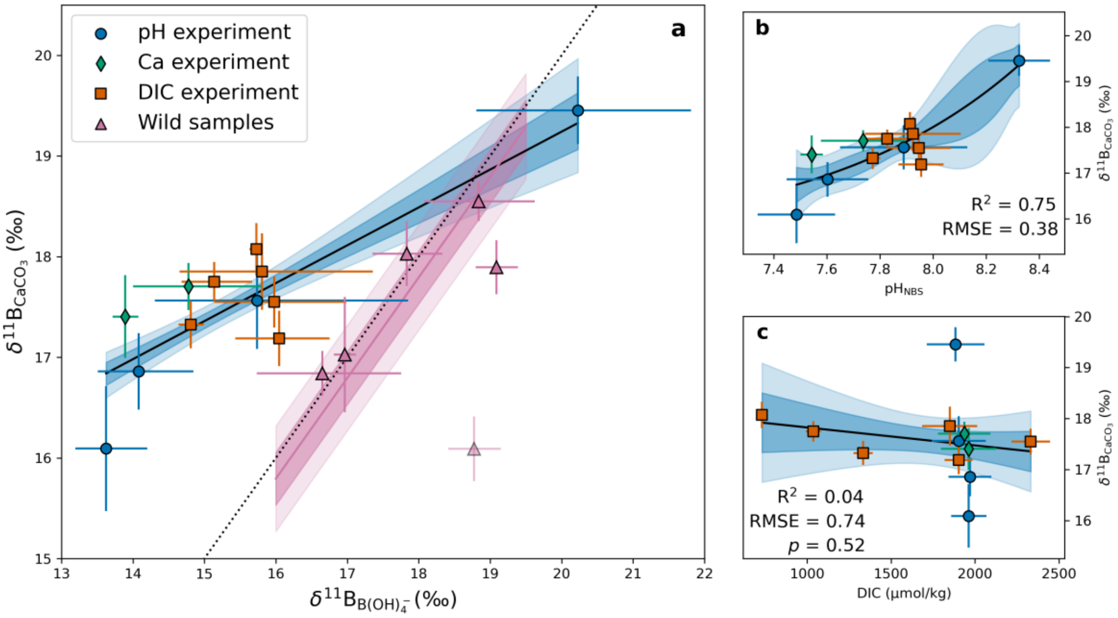

Figure 2: *Boron isotope calibration of Operculina ammonoides. (a) Regression between the measured $\delta^{11}B_{CaCO3}$ and calculated in-situ* $\delta^{11}B_{B(OH)4-}$. *Uncertainties are 2SE in the case of $\delta^{11}B_{CaCO3}$ and 2.5th and 97.5th percentiles of the Monte Carlo derived* $\delta^{11}B_{B(OH)4-}$ *(see text for details). The linear regression through the culture data was performed using a Monte Carlo approach by fitting a line through 10^5 data points randomly sampled from their uncertainty boundaries (blue regression). The displayed confidence region of the regression is the 16th / 84th (~1SD) and 2.5th / 97.5th (~2SD) percentiles of the predicted $\delta^{11}B_{CaCO3}$. The pink regression is fitted through the field samples with a forced slope of 1. (b) Logistic regression of $\delta^{11}B_{CaCO3}$ against weighted pH measurements. The p value was not reported because p values cannot be calculated on non-linear regressions. (c) Regression of $\delta^{11}B_{CaCO3}$ against DIC of jars.*

3.2 Comparison to other key proxy carriers

With a gradient of $0.38_{-0.10}^{+0.12}$ the calibration of cultured *Operculina ammonoides* appears to be one of the boron isotopic calibration of marine calcifiers with the shallowest slope when compared to previously published calibrations (Fig. 3). Although most of the previously published culture calibrations are less pH sensitive than $B(OH)_4^-$: *Amphistegina lobifera* (0.59 ± 0.28, Rollion-Bard and Erez, 2010), *Orbulina universa* (0.77 ± 0.07, Sanyal et al., 1996), *Trilobatus sacculifer (0.83 ± 0.07, Sanyal et al., 2001), Globigerinoides ruber (0.60 ± 0.08, Henehan et al., 2013),* only the calibration of *A. lobifera* has a gradient within uncertainty to that of cultured *O. ammonoides*.

However, previous calibrations of wild foraminfera specimens appear to be as pH sensitive as $B(OH)_4^-$: *Orbulina universa* (0.95 ± 0.17, Henehan et al., 2016), *Globigerina bulloides* (1.07 ± 0.25, Martínez-Botí et al., 2015) and the epifaunal deep benthic foraminifera *Cibicidoides wuellerstorfi*, *Cibicidoides mundulus* and *Planulina ariminensis* (Rae et al., 2011) which all lie on or in close vicinity to the boron isotopic composition of $B(OH)_4^-$. We also observe a similar trend when comparing the boron isotopic composition of cultured to wild *O. ammonoides* as they have a measured $\delta^{11}B_{CaCO3}$ closer to their estimated $\delta^{11}B_{B(OH)4-}$, except for the samples PD28 and SER.

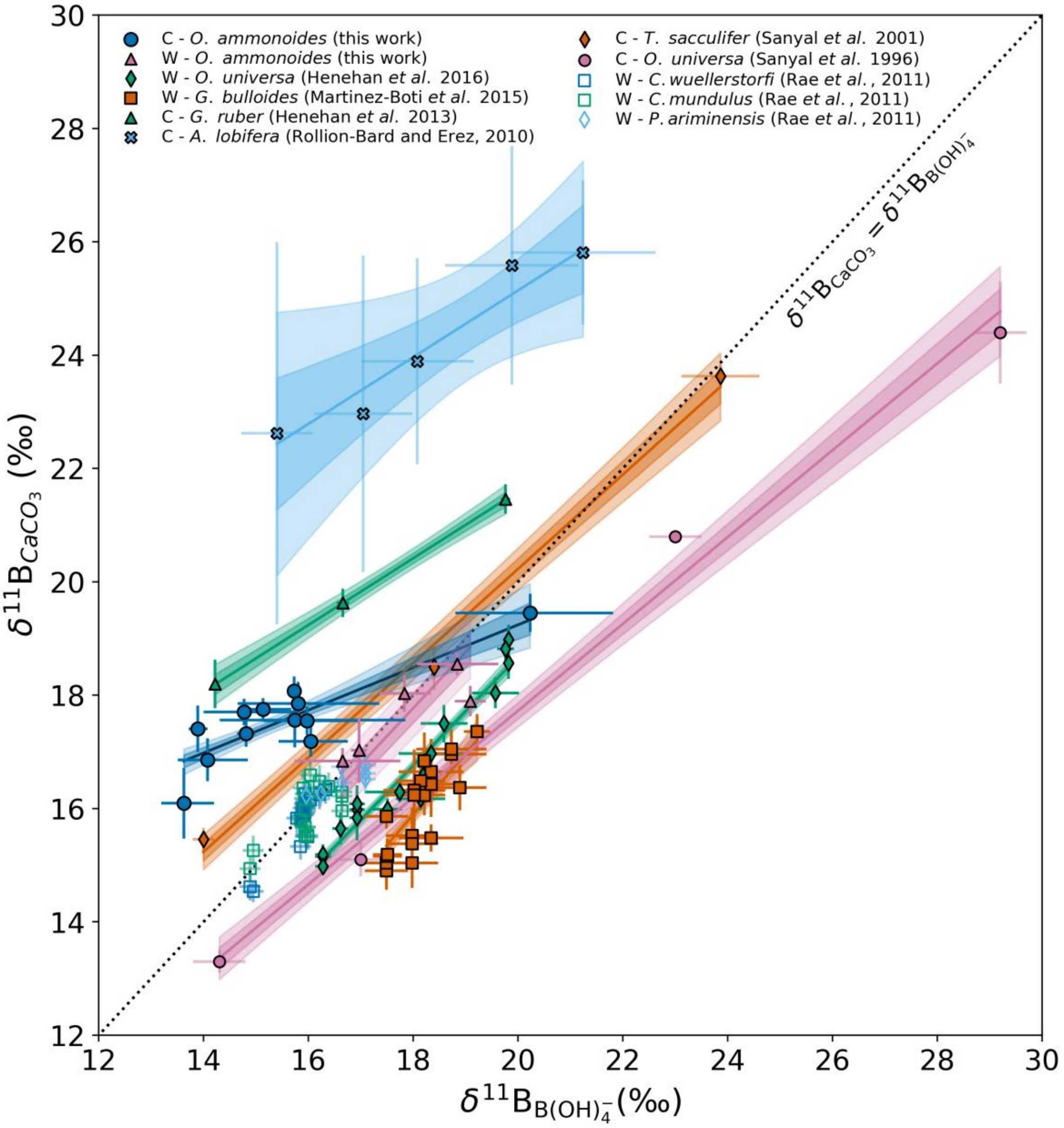

<u>Figure 3:</u> Comparison of the Operculina ammonoides boron isotope calibration presented here to previous studies. In-situ seawater $\delta^{11}B_{B(OH)4-}$ was calculated for the Amphistegina lobifera laboratory experiments using the information available in Rollion-Bard and Erez (2010) and the plotted $\delta^{11}B_{CaCO3}$ is the average and 2SD of each spot data. The linear regression fit and statistics are all calculated using a Monte Carlo approach, displayed uncertainty are thus different to the respective reported values. The first letter of the legend represents the origin the foraminifera used for the study, C = cultured and W = wild.

3.3 B/Ca

The B/Ca ratio is shown as a function of various aspects of calcite, seawater carbonate and boron chemistry to explore the possible influences on boron incorporation in *Operculina ammonoides.* The measured B/Ca of cultured *O. ammonoides* ranges between 211 and 454 μmol/mol (lowest and highest pH experiment, respectively). These concentrations are significantly higher than most planktonic foraminifera species (40-110 μmol/mol for a range of planktonic species, see Henehan et al., 2016 and references therein) and deep benthic foraminifera (120 to 200 μmol/mol, Rae et al., 2011) but close to other LBF estimates (*Amphistegina lessonii* and *Aphistegina lobifera*, 70 – 590 μmol/mol, Levi et al., 2019). We focus mainly on the possible relationship to $[B(OH)_4^-]$, since this is likely to be the dominant form of dissolved boron incorporated in the foraminifer's shell and therefore one of the main controls on the shell B/Ca (e.g. Hemming and Hanson, 1992; Klochko et al., 2009; Branson et al., 2015). However, because $B(OH)_4^-$ competes with CO_3^{2-} or HCO_3^- for the anion position in the lattice, controls on B/Ca may be best described by some combination of $B(OH)_4^-$ and either DIC, HCO_3^- or CO_3^{2-} (Allen et al., 2011; Foster, 2008; Haynes et al., 2017; Yu et al., 2007; Yu and Elderfield, 2007). Therefore we also explore the degree to which combined aspects of the seawater carbonate and boron systems can explain variations in *O. ammonoides* B/Ca.

We observe an extremely tight relationship between measured B/Ca and $\delta^{11}B_{CaCO3}$ (Fig. 4a, $R^2 = 0.91$, RSE= 0.24 ‰, $p = 7\cdot10^{-6}$). The weighted jar pH and the calculated $[B(OH)_4^-]$ (Fig. 4b and c) appear to explain a large portion of the variance in the B/Ca data, where $[B(OH)_4^-]$ shows a tighter relationship to measured B/Ca compared to pH. The B/Ca of *O. ammonoides* also has significant relationship with the $[B(OH)_4^-]/[DIC]$ ($R^2= 0.62$, RSE = 0.038 mmol/mol, p = 0.004). However, the B/Ca values from the constant pH, variable DIC experiment (Fig. 4d, orange squares) behave quite differently compared to the variable pH and $[Ca^{2+}_{SW}]$ experiments. The regression against $[B(OH)_4^-]/[DIC]$ is very similar to that of $[B(OH)_4^-]/[HCO_3^-]$ $^-$since HCO_3^- represents between 84% (pH_{NBS} = 8.32) and 95% (pH_{NBS} = 7.49) of the total DIC. This differs from planktonic foraminifera since it has been shown that the amount of boron incorporation in their shell appear to be not only sensitive to $[B(OH)_4^-]$, but also different components of the carbonate system (Allen et al., 2011, 2016; Haynes et al., 2017). The regression of B/Ca against $[B(OH)_4^-]/[CO_3^{2-}]$ shows no significant relationship ($R^2 = 0.023$, $p = 0.6$) when considering both variable pH and variable DIC experiments. However, when only considering the variable DIC experiment (HH7), with a wider

[CO_3^{2-}] range (45 and 157 μmol/mol), a tighter positive trend appears (Fig. 4e, starred statistics; R^2 = 0.63, RSE = 0.018 mmol/mol, p = 0.06).

The results of the PHREEQC simulations are shown in Figure 4f-i. This analysis shows that there is a significant relationship between B/Ca and the cation pairs $MgB(OH)_4^+$ (Fig. 4g) and $CaB(OH)_4^+$ (Fig. 4h) (R^2 = 0.67, p = 0.001, and R^2 = 0.74, p = 0.0004 respectively). The calculated $CaB(OH)_4^+$ concentration can explain more of the variance in the data compared to total $B(OH)_4^-$ (Fig. 4c), mainly because the experiments in which [$Ca^{2+}{}_{SW}$] was varied (HH6-5 and HH6-6, green diamonds in Fig. 4) have a higher [$CaB(OH)_4^+$] due to a higher [Ca^{2+}], bringing those two data points closer to the other the value of the other experiments with similar B/Ca. Similarly, when comparing [$B(OH)_4^-$]/[DIC] to the activity ratio of {$CaB(OH)_4^+$}/{HCO_3^-}, the trend remains nearly identical, but the fitting statistics are slightly better since the {$CaB(OH)_4^+$} values of the higher [$Ca^{2+}{}_{sw}$] experiments bring those two point closer to others, whilst the rest of the dataset remains similar (Fig. 4f). The regression between B/Ca and the activity of $B(OH)_4^-$ (Fig. 4i) is very similar to that alternatively using the bulk concentration of $B(OH)_4^-$ (Fig. 4c), suggesting that minor differences in the boron activity coefficients between the experiments cannot explain a substantial portion of the variance in the data.

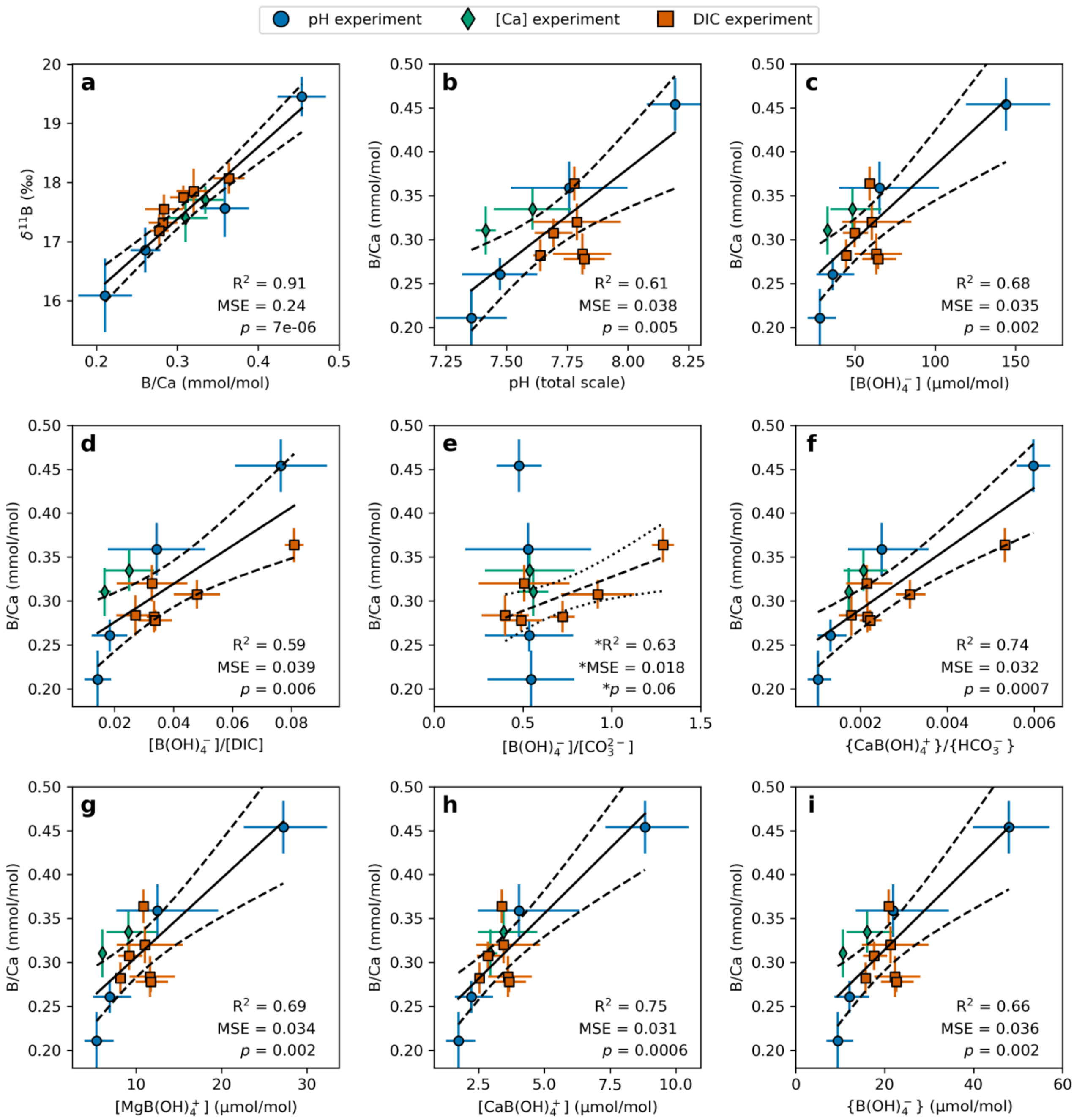

<u>Figure 4:</u> The relationship between Operculina ammonoides B/Ca and different aspects of the seawater carbon/boron system. (a) The regression of $\delta^{11}B_{CaCO3}$ and measured B/Ca is characterised by a significant linear relationship, hinting towards a common underlying driving factor. (b) Regression of B/Ca against the weighted pH of the culture jars. (c-e) Regression of B/Ca against aspects of the seawater carbonate and boron system calculated using PyCO2SYS. The regression between B/Ca and $[B(OH)_4^-]/[DIC]$, which potentially accounts for competition between carbon and boron species for the anion position in the lattice, appears slightly less significant than the concentration of $[B(OH)_4^-]$(c). (f-i) B/Ca regressions against the concentration and activity of key boron species calculated using PHREEQC. The linear regression between B/Ca and calculated $[B(OH)_4^-]/[CO_3^{2-}]$ (e) and given statistics only includes the DIC experiment (orange squares). The dotted lines represent the 2SD of the OLS fit. Linear regression statistics including the wild samples are available in the supplementary materials (Fig. S5).

4. Discussion:

4.1 Boron incorporation in *Operculina ammonoides*

Our results show that, the incorporation of boron into *Operculina ammonoides* is dominantly driven by the carbonate system, with $\delta^{11}B$ principally dependent on pH and B/Ca most closely correlated to $B(OH)_4^-$ or a borate-containing ion pair (Fig. 4).

Specifically, *O. ammonoides* B/Ca is most tightly correlated with the calculated $CaB(OH)_4^+$ ion pair concentration of seawater (R^2 = 0.75, MSE = 31 µmol/mol, $p = 6 \cdot 10^{-4}$; Fig. 4h), though we note that $CaB(OH)_4^+$ only results in a slightly better fit to the B/Ca data compared to $MgB(OH)_4^+$ and total $B(OH)_4^-$ (Fig. 4g and c). Indeed, the slightly improved fit based on $CaB(OH)_4^+$ or $CaB(OH)_4^+/HCO_3^-$ may well not imply mechanistic involvement of the Ca ion pair, since this cation pair modelling only affected the two calcium experiments HH6-5 and HH6-6 which were also conducted at slightly different average pH (green diamonds on Fig. 4). We note that Henehan et al. (2022) hypothesised that positively charged $CaB(OH)_4^+$ and $MgB(OH)_4^+$ ion pairs could migrate towards the growing crystal surface which has a negative electrostatic potential, repelling $B(OH)_4^-$ (Branson, 2018a), and warranting further study. However, we cannot robustly assess the potential involvement of the $MgB(OH)_4^+$ ion pair in boron incorporation because $[Mg^{2+}_{sw}]$ was similar in all experiments, such that the regression statistics when comparing B/Ca against $[MgB(OH)_4^+]$ and $[B(OH)_4^-]$ are nearly identical (Fig. 4g and c) as both parameters are driven by $[B(OH)_4^-]$.

It has also been hypothesized that the $NaB(OH)_4$ ion pair may play an important role in boron incorporation into calcite (Mavromatis et al., 2021). However, to our knowledge, no pitzer parameter exists for the $NaB(OH)_4$ ion pair, although a dissociation constant is available for the Minteq.v4 PhreeqC database (Pokrovski et al., 1995), which is intended for solutions with lower ionic strength (I<0.5, Allison et al., 1991). Consequently, we did not explore the possibility of $NaB(OH)_4$ as a driver of boron incorporation for *O. ammonoides*. Irrespective, there were no substantial changes in $[Na^+_{sw}]$ in our experiments, and unlike $[Ca^{2+}_{sw}]$ and $[Mg^{2+}_{sw}]$, $[Na^+_{sw}]$ varied by no more than a few percent during the Cenozoic (Zeebe and Tyrrell, 2019). As such, a $NaB(OH)_4^-$-B/Ca regression through our experimental data would almost certainly appear similar to $B(OH)_4^-$ versus B/Ca (Fig. 4c), which means that we cannot identify the importance or otherwise of this ion pair on foraminiferal boron uptake.

The measured B/Ca of the wild specimens fall within the range of the cultured *O. ammonoides* values (200 µmol/mol (SER) to 393 µmol/mol (SSO7G14)), but when compared to their respective $\delta^{11}B$ measurements not all follow the observed tight relationship of the culture experiments (Fig. S4). This may result from the fact that not all of these natural specimens were sampled live, such that not all lived at the same time and experienced the same seawater conditions. Given that the boron isotope and trace element measurements were not performed on the same specimens, it is also possible that geochemical heterogeneity within the sample population may be a source of bias in some cases, especially for samples from particularly variable environments. For example, PD28 (Renema, 2002) and SER (Renema, 2008) were sampled in reefs close to large cities (Makassar and Jakarta, respectively). Unlike for the sample KKE30 and BBX49a which we have pH measurements from nearby islands, we do not have pH data for PD28 nor SER samples. A local anthropogenic influence coupled with the use a of a coarse-resolution dataset (Gregor and Gruber, 2021) for the seawater physical and chemical properties might be an additional substantial source of uncertainty when interpreting data from these samples which are the most notable outliers (Fig. 4). However, we stress that this is not an issue for the majority of the dataset, as most wild specimens fall close to the linear regression between the different carbonate/boron system and B/Ca of the cultured material.

Overall, the B/Ca data strongly suggest that $[B(OH)_4^-]$ or a closely related parameter controls boron incorporation into this species both in the field and in laboratory cultures (Fig. 4). Given that is the case, in the next section we explore why our laboratory culture calibration of the relationship between $\delta^{11}B_{CaCO3}$ and $\delta^{11}B_{B(OH)4-}$ is characterised by a much shallower slope and more positive $\delta^{11}B_{CaCO3}$ values than samples collected from the field.

4.2 Low pH sensitivity of cultured *Operculina ammonoides*

The laboratory culture gradient of the relationship between measured $\delta^{11}B_{CaCO3}$ and *in situ* $\delta^{11}B_{B(OH)4-}$ is substantially lower than 1 (Fig. 2a), indicating that that some process other than seawater pH influences the boron isotopic composition of *Operculina ammonoides*. This has been observed in other culture calibrations of both benthic and planktonic symbiont bearing foraminifera (Rollion-Bard and Erez, 2010; Henehan et al., 2013). It has been previously shown that symbiont bearing planktonic foraminifera do alter their micro-environment considerably via a combination of calcification, respiration and photosynthesis (Jørgensen et al., 1985; Rink et al., 1998; Erez, 2003; Köhler-Rink and Kühl, 2005; Glas et al., 2012b). On one hand calcification and respiration acidifies the surrounding micro-environment of the calcifying organism, also known as the diffusive boundary layer (DBL) (Wolf-Gladrow et al., 1999; Zeebe and Wolf-Gladrow, 2001; Erez, 2003; Glas et al., 2012b, a; Toyofuku et al., 2017), whereas photosynthesis by the symbionts consumes

CO_2, raising the microenvironment pH (Erez, 2003; Glas et al., 2012a). In general, there is a net increase in pH in the DBL during the day since photosynthesis prevails over the acidifying effects of calcification and respiration (Rink et al., 1998; Köhler-Rink and Kühl, 2000, 2005; Oron et al., 2020). During the night, calcification and respiration continues while photosynthesis is shut off, leaving a net decrease in the pH of the DBL relative to bulk seawater. Since the rate of photosynthesis in cultured *O. ammonoides* is not impacted by changing pH or DIC (Oron et al., 2020), the pH increase during the day is relatively constant at different surrounding pH and DIC concentrations. In contrast, calcification rates decrease at lower seawater pH (Oron et al., 2020), such that, taken together, it is expected that the net pH elevation in the DBL of cultured *O. ammonoides* increases as seawater pH decreases.

This effect may be exacerbated in our experiments because the size of the DBL of the cultured *O. ammonoides* may have been larger compared to wild specimens since there was no water flow in the jars (Köhler-Rink and Kühl, 2000; Glas et al., 2012a; Toyofuku et al., 2017). Experiments from Köhler-Rink and Kühl (2000) showed that the size of the DBL of three LBF species (including a hyaline species) increased by a factor of four (from ~100 to ~400 µm) when there was no water flow, with an increase in DBL pH of ~0.2 between surrounding seawater and the foraminifer's surface when no flow was present. In our experiments, *O. ammonoides* were cultured in jars with ~10 days between water exchanges, such that they potentially had an even larger DBL. If *O. ammonoides* cultured in this way do indeed have a comparatively larger DBL, which is more alkaline at lower seawater pH as a result of their lower calcification rate under these conditions, then this might act as a strong dampening mechanism against changes in surrounding pH which could explain the shallower gradient observed in the boron isotope calibration.

Oron *et al.* (2020) also showed that *O. ammonoides* calcifies substantially more during the day than at night. Specifically, cultured *O. ammonoides* calcified 29 ± 7 % less on average in the dark. This means that, ~2/3 of the test of *O. ammonoides* should reflect calcification under light conditions, where photosynthesis results in a higher DBL pH, such that $\delta^{11}B_{B(OH)4-}$ in the boundary layer is more positive than that of the surrounding $\delta^{11}B_{B(OH)4-}$ especially at lower seawater pH values when calcification is inhibited.

The reduced size of the DBL by water flow/turbulence could explain why the field collected specimens appear to be more sensitive to pH, as their microenvironment is less impacted by the rates of calcification, respiration and photosynthesis. The low DBL size would then mean that the wild *O. ammonoides* would sample seawater with physical and chemical properties much closer to the overall surrounding seawater and not that of a heavily altered seawater. Although planktonic foraminifera have a different physiology, previous work seem to point towards this phenomenon. Indeed, most wild specimen calibration appear to be as pH sensitive as $B(OH)_4^-$, with gradients of ~1, while most culture calibrations appear to be less pH sensitive than $B(OH)_4^-$ (Fig. 3). Rae (2018) suggested that in some instances, such as the culture calibration of *Orbulina universa* of Sanyal et al., (1996), part of the offset to lower $\delta^{11}B$ at higher pH in cultures may be explained by a simple assumption of calcification rate varying as a function of $\Omega_{calcite}$, which has a wide range in some culture experiments (e.g. ~1.5 – 20 in Sanyal et al., 1996) compared to surface ocean waters (~4-7; e.g. Ridgwell 2005). This, in combination with the DBL diffusion effect described above, could drive the pH and $\delta^{11}B_{B(OH)4-}$ of the cultured microenvironment much lower than seawater at high pH, which would explain the greater deviation between the measured $\delta^{11}B_{CaCO3}$ and $\delta^{11}B_{B(OH)4-}$ of samples at higher pH in Sanyal et al. (1996) experiments. This shows that although some boron isotopes pH calibrations of cultured foraminifera display a low pH sensitivity, they can record faithfully $\delta^{11}B_{B(OH)4-}$, but that of a more heavily altered micro-environment, which may not be applicable to wild specimens. That is why we will explore, in the next session, a way of modelling the DBL of cultured *O. ammonoides* to explore possible influences which would result in a shallower calibration that we observed.

4.3 Micro-environment modelling

The processes of photosynthesis, respiration and calcification create concentration gradients in O_2, DIC, Ca^{2+} and pH between the bulk seawater and the surface of the shell (Jørgensen et al., 1985; Rink et al., 1998; Köhler-Rink and Kühl, 2000, 2005; Glas et al., 2012b, a). Given the equilibrium values of the chemical reaction constants and known diffusion rates of each dissolved species, which are also dependant on the physical properties of seawater (Dickson et al., 2007), the concentration profiles of each species can be calculated as a function of distance from the surface of the foraminifera for a given rate in the three key aforementioned processes. Here, we use a diffusion-reaction model to understand the degree to which the chemistry of the seawater close to the shell surface might depend on DBL thickness in cultured *Operculina ammonoides*. We stress that we do so to determine whether the offsets that we observe between $\delta^{11}B_{CaCO3}$ and *in situ* $\delta^{11}B_{B(OH)4-}$ are of the magnitude that we might expect given a pH-dependent change in calcification rate, rather than to constrain the necessary rates of these processes and/or DBL thickness required to explain the details of our dataset. Such a model was developed by Wolf-Gladrow et al. (1999), and later updated by Zeebe et al. (2003) to include isotopes of boron. This model requires the following inputs: foraminifera geometry, seawater physical and chemical parameters (temperature, salinity, pH, alkalinity or DIC) and carbon fluxes at the surface of the foraminifera, appropriate values of which were determined as follows:

1. This reaction-diffusion model was designed with spherical geometry of certain planktonic foraminifera in mind (e.g. *Orbulina universa*). While *Operculina ammonoides* (and other LBF) are closer to an oblate spheroid than a sphere (Renema, 2002; Hohenegger, 2018), the specific geometry of the foraminifer matters little here as the sensitivity of DBL chemistry to the fluxes in the model mainly depends on surface area. Oron et al. (2018) measured the surface area of involute and evolute *O. ammonoides* from the Gulf of Eilat/Aqaba as a function of shell weight, which we couple with shell weight measurements available from all the laboratory cultured foraminifera studied here. Because the reaction-diffusion model needs a radius as input (since it assumes spherical geometry), the closest spherical area to the estimated area from weight measurement was used to calculate the radius of that hypothetical sphere to be used as the model input.

2. The key seawater parameters (i.e. pH and DIC, the latter calculated from TAlk) were taken from the weighted mean measurements of the culture jars, as these represent our best assessment of the average conditions experienced by the cultured foraminifera (see section 2.2).

3. The carbon fluxes at the surface of the foraminifera were estimated by calculating the photosynthesis, respiration and calcification rates following Oron et al. (2020). The rate of calcification was calculated using the alkalinity depletion of the culture jars (see supplements). The alkalinity depletion of the jars over the course of 30 days was converted to calcification rate using Eq. 2 of Oron et al. (2020). A one-month timespan was chosen as most growth took place in the first part of the experiments (Fig. S2d). Photosynthesis and respiration were estimated using Eq. 3 of Oron et al. (2020). This approach is based on the fact that DIC decreases when photosynthesis takes place (in the form of CO_2) and increases during respiration, the balance of which will be reflected in the jar DIC over the course of 10 days. DIC drawdown via calcification was taken into account by subtracting half of the alkalinity drawdown. Unlike the spinose planktonic foraminifera, *O. ammonoides* (and other LBF) retain their symbionts within the cytoplasm, underneath the shell (Hansen and Buchardt, 1977). For the purposes of the model, it was assumed that all fluxes took place directly at the surface of the shell, but we acknowledge this as a caveat because the chemistry alteration due to photosymbionts in *O. ammonoides* should then remain internal, but this issue will be discussed further later in this section.

We applied this model to all experiments, however, the calcification and photosynthesis / respiration (P/R) rate of HH7 and HH6 differ greatly. The HH6 experiments (variable pH and

[Ca_{sw}]) have an average P/R rate of 2.88 ± 0.32 nmol C/h/individual (2SD) while the HH7 experiments (variable DIC) have an average P/R rate of 0.80 ± 0.79 nmol C/h/individual (2SD). Although it has been found that P/R rate in *O. ammonoides* are relatively constant across different seawater pH or DIC (Oron et al., 2020), the estimated P/R rates of the cultured *O. ammonoides* in HH7 has a high variability and is significantly lower than the estimations for the *O. ammonoides* in the HH6 experiment set (Fig. S8). In spite of being grown at normal seawater pH, the *O. ammonoides* in the HH7 experiments also did calcify significantly less than the *O. ammonoides* in the HH6 experiments (Fig. S8).

One of the reasons to explain why the difference in calcification rates between the two experiment sets is, as mentioned in section 2.1, the *O. ammonoides* sampled for the HH6 experiments were sieved between the 350 and 475 µm while the *O. ammonoides* sampled for the HH7 experiments were sieved between 475 and 690 µm. It has been shown that the average rate of calcification of cultured *O. ammonoides* is inversely proportional to its size (Oron et al., 2020), and so the larger foraminifera used for the HH7 experimental had calcified less than their smaller counterpart in the HH6 experimental set. However, this would not explain why the P/R rates of the foraminifera grown in HH7 were significantly lower than those in the HH6 experiments. We note that we have no direct knowledge of whether or not calcification was a discontinuous process during these experiments, such that we can only determine an average rate of calcification; for this reason we use the model to assess the direction and approximate magnitude of likely DBL chemistry changes, but do not attempt to explain the dataset in detail using this approach. To compare our estimates of DBL pH with the boron isotopic composition of the shell, we make the simplifying assumption that only borate ion is incorporated into the calcite precipitated by this species, and that this borate ion has the isotopic composition of borate ion in the DBL. From this, we can calculate pH in the DBL from our shell $\delta^{11}B$ values and compare it to the model output.

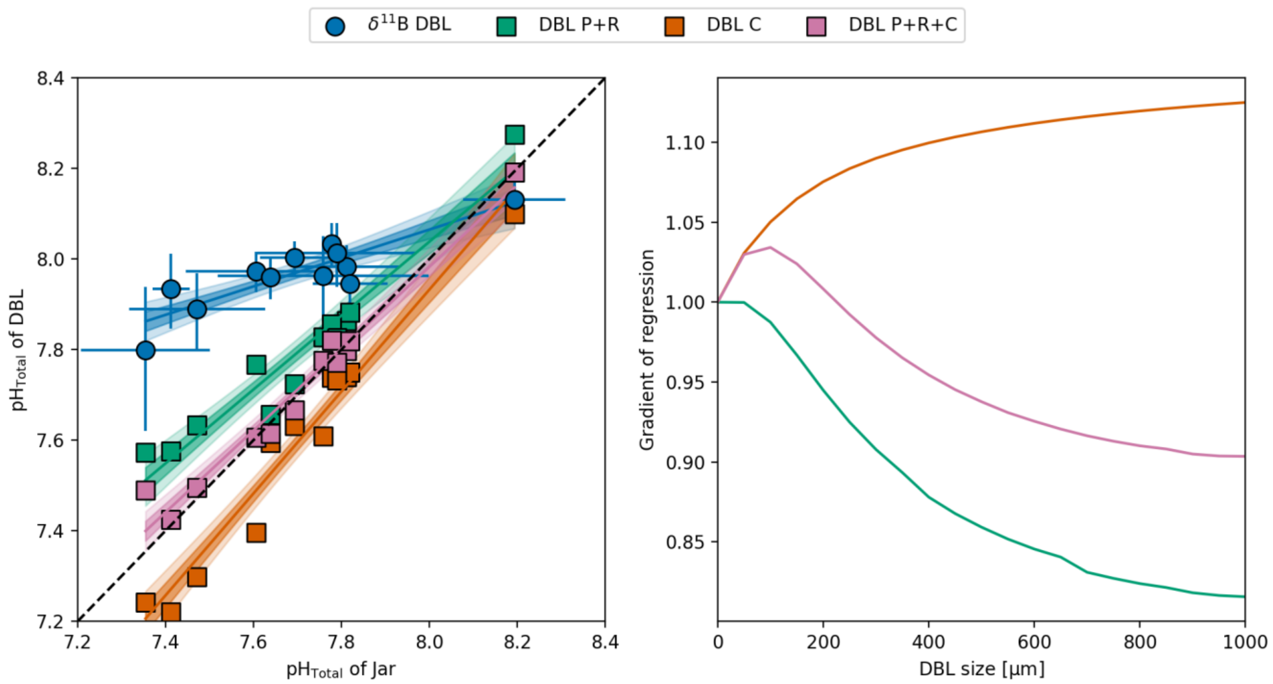

Figure 5: Modelled and estimated pH of Operculina ammonoides micro-environment. (a) Estimated pH of DBL as a function of weighted jar pH. The pH reconstructed using $\delta^{11}B_{CaCO3}$ was made using the assumption of $\delta^{11}B_{CaCO3}$ = $\delta^{11}B_{B(OH)4-}$ (see text). The calculation was done using the Monte Carlo simulated $\delta^{11}B_{B(OH)4-}$ and convert it to pH using the calculated pK_b^* and updated equation from Rae (2018). The displayed points are the median of the Monte Carlo datasets and the uncertainties are the 2.5th and 97.5th percentiles. The dashed line represents the 1:1 line. The different coloured squares represent the modelled pH of the DBL at the surface of the foraminifera. The key to the legend is as follows: P = photosynthesis, R = respiration, C = calcification. In green, the fluxes at the surface was modelled to only consider the balance between photosynthesis and respiration, in orange, only calcification and in pink the balance between the previous two. All fluxes were estimated using culutre jars chemistry (see text). An OLS regression was calculated for each simulation and the 1 and 2SD of the fit is displayed as the shaded region. A DBL size of 1000 μm was used for the model. (b) Gradients of the OLS fit between modelled micro-environment pH and pH of culturing medium as a function of DBL size. The fluxes were kept the same as in panel (a) and only the size of the DBL was changed. The colours of the lines follow the same colour code as panel (a).

The diffusion-reaction model allows the different fluxes to be selectively added or removed to study their individual and combined impact on the seawater chemistry of the DBL (Fig. 5). Figure 5a shows the reconstructed pH at the surface of the foraminifera both from the diffusion-reaction model and the measured boron isotopes (assuming $\delta^{11}B_{CaCO3}$ = $\delta^{11}B_{B(OH)4-}$) as a function of mean culture jar pH experienced by the foraminifera (weighted average of pH). All experiments but the highest pH experiment (HH6-4: $pH_T \approx 8.20$) are characterised by a boron isotopic signature indicative of a pH significantly higher than surrounding seawater. The estimated surface pH from the measured $\delta^{11}B$ of the shell of these experiments are closer to the photosynthesis driven modelled micro-environment. Inversely, the higher pH experiment (HH6-4: $pH_T \approx 8.20$) seems to record a micro-environment pH closer to a modelled DBL dominated by calcification. A similar observation was made by Rae (2018) when modelling the micro-environment $\delta^{11}B_{B(OH)4-}$ of the cultured *Orbulina universa* of Sanyal et al. (1996), finding that the higher pH experiments were characterised by $\delta^{11}B_{CaCO3}$ close to modelled $\delta^{11}B_{B(OH)4-}$ when scaling calcification with $\Omega_{calcite}$. Although we note that the reconstructed DBL pH of the lower pH experiments is not within the uncertainty to the modelled pH.

By varying the size of the DBL and keeping the carbon fluxes and the geometry constant, we can investigate how the pH of seawater at the surface of the foraminifera responds to an increasingly reaction driven flux of carbon at the surface. As an example, Figure 5b shows the variation of the gradient of linear regression between reconstructed DBL pH and pH of the culture medium (as illustrated in Fig. 5a) as a function of DBL size under different carbon flux scenario. The distinction in regression gradient between a calcification only and P/R only scenario becomes noticeable after a DBL size of few hundred µm, after which the difference increases until it reaches a pseudo-plateau (Fig. 5b). In the case of the lowest pH experiment (HH6-1), it has a calculated average P/R rate of ~3.32 nmol C/h/individual while it has a calculated average calcification rate of ~0.81 nmol C/h/individual. In this case, the consumption of CO_2 outweighs its release in the DBL and so the pH at the surface of the foraminifera will be higher than the surrounding seawater. When the DBL is larger, the surface of the cultured foraminifera would be more depleted in CO_2, but because diffusion happens more slowly than the flux of carbon at the surface, the main CO_2 source would be from the re-equilibration of HCO_3^-, which would consume a proton and further increase pH. Inversely, when the DBL is smaller, CO_2 readily diffuses to replenish the surface layer, and thus the surface pH increase is less pronounced. In the case of the highest pH experiment (HH6-4), it has an estimated photosynthesis rate of ~3.32 nmol C/h/individual and is close to the calculated average rate of calcification (~3.57 nmol C/h/individual). Unlike HH6-1, there is a net release of CO_2 in the DBL and the seawater at the surface of the foraminifera will be more acidic. This explains why, when combining all the fluxes (pink squares), the resulting surface pH of the DBL is close to the surrounding seawater pH, since the fluxes broadly cancel out. After a certain DBL size, the changes in micro-environment pH plateau as the DBL becomes increasingly reaction driven rather than diffusion dominated, ultimately reaching a quasi-equilibrium at a size of ~1000 µm.

The diffusion-reaction model of the micro-environment presented here describes the chemistry of seawater in the DBL for fluxes averaged over a period of weeks, such that it is important to note that the model cannot capture the variability of these fluxes through time. For example, calcification is likely not a continuous process like respiration but a discrete event lasting a few hours every few days (Erez, 2003; Glas et al., 2012b), the timing of which is difficult to constrain on a population level. This could mean that during a calcification event, the decrease in the DBL pH would be stronger and thus record a boron isotopic composition lower than predicted, although comparing the calculated DBL pH from $\delta^{11}B_{CaCO3}$ to the model would not support this (Fig. 5). In addition, we note that genus *Operculina* is likely similar to other hyaline tropical benthic species, in that it probably possesses an internal carbon pool and vacuolises seawater (ter Kuile and Erez, 1987; Erez, 2003; Bentov et al., 2009; De Nooijer et al., 2009; Evans et al., 2018). This means that the process of chamber formation could be decoupled from the time at which seawater is vacuolised from around the organism. While there is evidence for light enhanced calcification (Erez, 2003; Oron et al., 2020) and respiration (Erez, 2003), hinting towards enhanced metabolic activity during the day, we cannot quantify their respective effects on the incorporation of boron in *O. ammonoides*. There is also evidence in hyaline foraminifera that the residence time of vacuolised seawater within the foraminifera can vary from less than 1 hour (during calcification) to more than 48h (outside of calcification) (Bentov et al., 2009). Hyaline foraminifera are also characterised by a dense pseudopodia network in proximity to their shell surface which perform some of the life functions of the foraminifera namely feeding, respiration, movement, chamber formation and excretion (Erez, 2003). Doing this, pseudopodia also alter the micro-environment of the LBF, although we cannot quantify this modification. The pseudopodia are also responsible for some of the seawater vacuolisation by the foraminifera, which might be sampled from further away from the shell's surface (Erez, 2003; Bentov et al., 2009). The vacuolised seawater will undergo a strong pH increase until it reaches the site of calcification (De Nooijer et al., 2008, 2009), but the boron isotopic composition recorded by *O. ammonoides* (and other foraminifera) usually sits closer to $\delta^{11}B_{B(OH)4-}$ at their respective seawater pH (see Fig. 4) and not at around 25 or 30 ‰ which would be the $\delta^{11}B_{B(OH)4-}$ of the alkalinised vacuoles or calcifying fluid (pH ≈ 9). It has been hypothesised that boric acid, permeating through membranes, would isotopically equilibrate the calcifying fluid with the surrounding seawater (Gagnon et al., 2021). If the calcifying fluid is isotopically equilibrated with the surrounding altered DBL, it would allow the precipitated calcite to record the $\delta^{11}B_{B(OH)4-}$ of the altered DBL.

Operculina ammonoides lives near the shallow reef base habitat (Hohenegger et al., 1999; Renema, 2002), which are comparatively higher-energy environments compared to the quiescence of laboratory cultures. Previous experiments which introduced a unidirectional flow to the culture bath, measured a DBL thickness to be around 100 µm (vertical dashed line in Fig. 5b) in hyaline

LBF (Köhler-Rink and Kühl, 2000; Glas et al., 2012a). At this size, the diffusion reaction model predicts very modest changes compared to the bulk seawater, ranging from 0.03 units (HH6-4) to 0.05 units (HH6-1) in either P/R only or calcification only scenario. This modelled non-significant alteration for wild specimens could tentatively explain their $\delta^{11}B_{CaCO3}$ being closer to their calculated $\delta^{11}B_{B(OH)4-}$, but it does hint to a mechanism to explain the offset that we observe between field and laboratory cultured specimens grown at similar seawater pH and the difference in the nature of their sensitivity to $\delta^{11}B_{B(OH)4-}$.

In summary, the DBL diffusion-reaction model results demonstrate that carbonate chemistry in the boundary layer is strongly sensitive to the DBL thickness for fluxes relevant to *Operculina ammonoides*. The results are consistent with a boundary layer pH lower than ambient seawater for a likely DBL thickness in the natural environment, if calcification and/or respiration rates are higher relative to photosynthesis than those measured in the laboratory. In contrast, a thicker DBL in the laboratory coupled with a DBL dominated by photosynthesis highlights mechanistic differences between field-collected and laboratory cultured $\delta^{11}B_{CaCO3}$ values at a given pH (Fig. 2), and the shallow $\delta^{11}B_{CaCO3}$-$\delta^{11}B_{B(OH)4-}$ slope observed in cultured specimens.

5. Conclusions:

Here, we show how the use of LA-MC-ICPMS to selectively sample calcite precipitated during controlled laboratory culture experiments allows the relationship between the boron isotopic composition of the shell and pH to be calibrated for larger benthic foraminifera. We show that cultured *Operculina ammonoides* is characterised by a $\delta^{11}B_{CaCO3}$-$\delta^{11}B_{B(OH)4-}$ slope substantially lower than 1. In contrast, wild-collected specimens have a measured boron isotopic composition close to their calculated *in-situ* $B(OH)_4^-$. We explored this discrepancy using a previously published diffusion-reaction model (Wolf-Gladrow et al., 1999), the results of which show that cultured *O. ammonoides* may be characterised by a shallow $\delta^{11}B_{CaCO3}$-$\delta^{11}B_{B(OH)4-}$ slope as a result of a strongly altered micro-environment because of a thick diffuse boundary layer in the quiescent laboratory culture conditions compared to specimens growing in the wild. Future culture studies should therefore be mindful of potential differences in the micro-environment of foraminifera between the laboratory and field, especially when interpreting geochemical data in the light of carbonate/boron seawater chemistry. In addition, B/Ca data show that boron incorporation in *O. ammonoides* is dominantly controlled by some aspect of seawater borate chemistry (e.g. $[B(OH)_4^-]$ or a borate ion pair). This potentially paves the way forward for coupling this information to boron isotope measurements in order to constrain calcification site or seawater carbonate chemistry. More broadly, our results demonstrate that the nummulitid tropical shallow-dwelling foraminifera are a useful group of calcifiers for paleo-pH/CO_2 reconstruction using the data presented here, especially given that some genera, such as *Operculina* are present throughout the majority of the Cenozoic.

Acknowledgements:

We thank Richard Zeebe and Dieter Wolf-Gladrow for providing their code for their diffusion-reaction model and Oscar Branson for providing the Python frontend. We thank Khan Phita at the UNHAS in Makassar, Indonesia, for providing the seawater pH measurements of island reefs near Makassar used for the sample KKE30. FIERCE is financially supported by the Wilhelm and Else Heraeus Foundation and by the Deutsche Forschungsgemeinschaft (DFG: INST 161/921-1 FUGG, INST 161/923-1 FUGG and INST 161/1073-1 FUGG), which is gratefully acknowledged. This research was funded through the VeWA research consortium (Past Warm Periods as Natural Analogues of our high-CO_2 Climate Future) by the LOEWE programme of the Hessen Ministry of Higher Education, Research and the Arts, Germany.

Data availability

Data are available through Zenodo at https://[URL].

References

Allen K. A., Hönisch B., Eggins S. M., Haynes L. L., Rosenthal Y. and Yu J. (2016) Trace element proxies for surface ocean conditions: A synthesis of culture calibrations with planktic foraminifera. *Geochim. Cosmochim. Acta* **193**, 197–221.

Allen K. A., Hönisch B., Eggins S. M., Yu J., Spero H. J. and Elderfield H. (2011) Controls on boron incorporation in cultured tests of the planktic foraminifer Orbulina universa. *Geophys. Res. Lett.* **309**, 291–301.

Allison J. D., Brown D. S. and Novo-Gradac K. J. (1991) *MINTEQA2/PRODEFA2, a Geochemical Assessment Model for Environmental Systems: Version 3.0 User's Manual.*, Environmental Research Laboratory, Office of Research and Development, U.S. Environmental Protection Agency.

Anagnostou E., Huang K.-F., You C.-F., Sikes E. L. and Sherrell R. M. (2012) Evaluation of boron isotope ratio as a pH proxy in the deep sea coral Desmophyllum dianthus: Evidence of physiological pH adjustment. *Earth Planet. Sci. Lett.* **349–350**, 251–260.

Anagnostou E., John E. H., Edgar K. M., Foster G. L., Ridgwell A., Inglis G. N., Pancost R. D., Lunt D. J. and Pearson P. N. (2016) Changing atmospheric CO2 concentration was the primary driver of early Cenozoic climate. *Nature* **533**, 380–384.

Barker S., Greaves M. and Elderfield H. (2003) A study of cleaning procedures used for foraminiferal Mg/Ca paleothermometry. *Geochem. Geophys. Geosystems* **4**.

Bentov S., Brownlee C. and Erez J. (2009) The role of seawater endocytosis in the biomineralization process in calcareous foraminifera. *Proc. Natl. Acad. Sci.* **106**, 21500–21504.

Branson O. (2018a) Chapter 4: Boron incorporation into marine CaCO 3. In *Boron Isotopes* (eds. H. Marshall ang G. Foster). Springer. pp. 71–105.

Branson O. (2018b) oscarbranson/cbsyst: 0.4.5. https://doi.org/10.5281/zenodo.7620872. Accessed: 2023-02-08.

Branson O., Kaczmarek K., Redfern S. A. T., Misra S., Langer G., Tyliszczak T., Bijma J. and Elderfield H. (2015) The coordination and distribution of B in foraminiferal calcite. *Earth Planet. Sci. Lett.* **416**, 67–72.

Cotton L. J., Evans D. and Beavington-Penney S. J. (2020) The high-magnesium calcite origin of Nummulitd foraminifera and implications for the identification of calcite diagenesis. *PALAIOS* **35**, 421–431.

D'Agostino R. and Pearson E. S. (1973) Tests for departure from normality. Empirical results for the distributions of b2 and sqrt b1. *Biometrika* **60**, 613–622.

De Nooijer L. J., Toyofuku T. and Kitazato H. (2009) Foraminifera promote calcification by elevating their intracellular pH. *Proc. Natl. Acad. Sci.* **106**, 15374–15378.

De Nooijer L. J., Toyofuku T., Oguri K., Nomaki H. and Kitazato H. (2008) Intracellular pH distribution in foraminifera determined by the fluorescent probe HPTS: Intracellular pH of foraminifera. *Limnol. Oceanogr. Methods* **6**, 610–618.

Dickson A. G. (1990) Thermodynamics of the dissociation of boric acid in synthetic seawater from 273.15 to 318.15 K. *Deep Sea Res. Part Oceanogr. Res. Pap.* **37**, 755–766.

Dickson A. G., Sabine C. L., Christian J. R., Bargeron C. P. and North Pacific Marine Science Organization eds. (2007) *Guide to best practices for ocean CO2 measurements*., North Pacific Marine Science Organization, Sidney, BC.

Edwards K. J. and Valley J. W. (1998) Oxygen isotope diffusion and zoning in diopside: the importance of water fugacity during cooling. *Geochim. Cosmochim. Acta* **62**, 2265–2277.

Erez J. (2003) The Source of Ions for Biomineralization in Foraminifera and Their Implications for Paleoceanographic Proxies. *Rev. Mineral. Geochem.* **54**, 115–149.

Evans D., Brierley C., Raymo M. E., Erez J. and Müller W. (2016) Planktic foraminifera shell chemistry response to seawater chemistry: Pliocene–Pleistocene seawater Mg/Ca, temperature and sea level change. *Earth Planet. Sci. Lett.* **438**, 139–148.

Evans D., Erez J., Oron S. and Müller W. (2015) Mg/Ca-temperature and seawater-test chemistry relationships in the shallow-dwelling large benthic foraminifera Operculina ammonoides. *Geochim. Cosmochim. Acta* **148**, 325–342.

Evans D., Gerdes A., Coenen D., Marschall H. R. and Müller W. (2021) Accurate correction for the matrix interference on laser ablation MC-ICPMS boron isotope measurements in CaCO3 and silicate matrices. *J. Anal. At. Spectrom.* **36**, 1607–1617.

Evans D. and Müller W. (2018) Automated Extraction of a Five-Year LA-ICP-MS Trace Element Data Set of Ten Common Glass and Carbonate Reference Materials: Long-Term Data Quality, Optimisation and Laser Cell Homogeneity. *Geostand. Geoanalytical Res.* **42**, 159–188.

Evans D., Müller W. and Erez J. (2018) Assessing foraminifera biomineralisation models through trace element data of cultures under variable seawater chemistry. *Geochim. Cosmochim. Acta* **236**, 198–217.

Evans D., Müller W., Oron S. and Renema W. (2013) Eocene seasonality and seawater alkaline earth reconstruction using shallow-dwelling large benthic foraminifera. *Earth Planet. Sci. Lett.* **381**, 104–115.

Farmer J. R., Branson O., Uchikawa J., Penman D. E., Hönisch B. and Zeebe R. E. (2019) Boric acid and borate incorporation in inorganic calcite inferred from B/Ca, boron isotopes and surface kinetic modeling. *Geochim. Cosmochim. Acta* **244**, 229–247.

Foster G. L. (2008) Seawater pH, pCO2 and [CO2-3] variations in the Caribbean Sea over the last 130 kyr: A boron isotope and B/Ca study of planktic foraminifera. *Earth Planet. Sci. Lett.* **271**, 254–266.

Foster G. L. and Rae J. W. B. (2016) Reconstructing Ocean pH with Boron Isotopes in Foraminifera. *Annu. Rev. Earth Planet. Sci.* **44**, 207–237.

Foster G. L., Strandmann P. A. E. P. von and Rae J. W. B. (2010) Boron and magnesium isotopic composition of seawater. *Geochem. Geophys. Geosystems* **11**.

Gagnon A. C., Gothmann A. M., Branson O., Rae J. W. B. and Stewart J. A. (2021) Controls on boron isotopes in a cold-water coral and the cost of resilience to ocean acidification. *Earth Planet. Sci. Lett.* **554**, 116662.

Gatz D. F. and Smith L. (1995) The standard error of a weighted mean concentration—I. Bootstrapping vs other methods. *Atmos. Environ.* **29**, 1185–1193.

Glas M. S., Fabricius K. E., Beer D. de and Uthicke S. (2012a) The O2, pH and Ca2+ microenvironment of benthic foraminifera in a high CO2 world ed. J. A. Gilbert. *PLOS ONE* **7**, e50010.

Glas M. S., Langer G. and Keul N. (2012b) Calcification acidifies the microenvironment of a benthic foraminifer (Ammonia sp.). *J. Exp. Mar. Biol. Ecol.* **424–425**, 53–58.

Graham C. M. and Wada H. (1998) Timescales and mechanisms of fluid infiltration in a marble: an ion microprobe study. *Contrib Miner. Pet.* **132**, 371–389.

Gregor L. and Gruber N. (2021) OceanSODA-ETHZ: a global gridded data set of the surface ocean carbonate system for seasonal to decadal studies of ocean acidification. *Earth Syst. Sci. Data* **13**, 777–808.

Gutjahr M., Bordier L., Douville E., Farmer J., Foster G. L., Hathorne E. C., Hönisch B., Lemarchand D., Louvat P., McCulloch M., Noireaux J., Pallavicini N., Rae J. W. B., Rodushkin I., Roux P., Stewart J. A., Thil F. and You C.-F. (2020) Sub-Permil Interlaboratory Consistency for Solution-Based Boron Isotope Analyses on Marine Carbonates. *Geostand. Geoanalytical Res.* **45**, 59–75.

Hain M. P., Sigman D. M., Higgins J. A. and Haug G. H. (2018) Response to Comment by Zeebe and Tyrrell on "The Effects of Secular Calcium and Magnesium Concentration Changes on the Thermodynamics of Seawater Acid/Base Chemistry: Implications for the Eocene and Cretaceous Ocean Carbon Chemistry and Buffering." *Glob. Biogeochem. Cycles* **32**, 898–901.

Hain M. P., Sigman D. M., Higgins J. A. and Haug G. H. (2015) The effects of secular calcium and magnesium concentration changes on the thermodynamics of seawater acid/base chemistry: Implications for Eocene and Cretaceous ocean carbon chemistry and buffering. *Glob. Biogeochem. Cycles* **29**, 517–533.

Hansen H. J. and Buchardt B. (1977) Depth distribution of Amphistegina in the Gulf of Eilat, Israel. *Utrecht Micropaleont Bull* **15**, 205–224.

Hathorne E. C., Gagnon A., Felis T., Adkins J., Asami R., Boer W., Caillon N., Case D., Cobb K. M., Douville E., deMenocal P., Eisenhauer A., Garbe-Schönberg D., Geibert W., Goldstein S., Hughen K., Inoue M., Kawahata H., Kölling M., Cornec F. L., Linsley B. K., McGregor H. V., Montagna P., Nurhati I. S., Quinn T. M., Raddatz J., Rebaubier H., Robinson L., Sadekov A., Sherrell R., Sinclair D., Tudhope A. W., Wei G., Wong H., Wu H. C. and You C.-F. (2013) Interlaboratory study for coral Sr/Ca and other element/Ca ratio measurements. *Geochem. Geophys. Geosystems* **14**, 3730–3750.

Hauzer H. (2022) Development of new foraminiferal proxies for paleochemistry of the oceans. The Hebrew University of Jerusalem.

Hauzer H., Evans D., Müller W., Rosenthal Y. and Erez J. (2018) Calibration of Na partitioning in the calcitic foraminifer Operculina ammonoides under variable Ca concentration: Toward reconstructing past seawater composition. *Earth Planet. Sci. Lett.* **497**, 80–91.

Hauzer H., Evans D., Müller W., Rosenthal Y. and Erez J. (2021) Salinity Effect on Trace Element Incorporation in Cultured Shells of the Large Benthic Foraminifer Operculina a mmonoides. *Paleoceanogr. Paleoclimatology* **36**.

Haynes L. L., Hönisch B., Dyez K. A., Holland K., Rosenthal Y., Fish C. R., Subhas A. V. and Rae J. W. B. (2017) Calibration of the B/Ca proxy in the planktic foraminifer Orbulina universa to Paleocene seawater conditions: Paleocene B/Ca in Cultured Orbulina universa. *Paleoceanography* **32**, 580–599.

Heinrich C. A., Pettke T., Halter W. E., Aigner-Torres M., Audétat A., Günther D., Hattendorf B., Bleiner D., Guillong M. and Horn I. (2003) Quantitative multi-element analysis of minerals, fluid and melt inclusions by laser-ablation inductively-coupled-plasma mass-spectrometry. *Geochim. Cosmochim. Acta* **67**, 3473–3497.

Hemming N. G. and Hanson G. N. (1992) Boron isotopic composition and concentration in modern marine carbonates. *Geochim. Cosmochim. Acta* **56**, 537–543.

Henehan M. J., Foster G. L., Bostock H. C., Greenop R., Marshall B. J. and Wilson P. A. (2016) A new boron isotope-pH calibration for Orbulina universa, with implications for understanding and accounting for `vital effects'. *Earth Planet. Sci. Lett.* **454**, 282–292.

Henehan M. J., Gebbinck C. D. K., Wymans J. V. B., Hain M. P., Rae J. W. B., Hönisch B., Foster G. L. and Kim S.-T. (2022) No ion is an island: Multiple ions influence boron incorporation into CaCO3. *Geochim. Cosmochim. Acta* **318**, 510–530.

Henehan M. J., Rae J. W. B., Foster G. L., Erez J., Prentice K. C., Kucera M., Bostock H. C., Martínez-Botí M. A., Milton J. A., Wilson P. A., Marshall B. J. and Elliott T. (2013) Calibration of the boron isotope proxy in the planktonic foraminifera Globigerinoides ruber for use in palaeo-CO2 reconstruction. *Earth Planet. Sci. Lett.* **364**, 111–122.

Hohenegger J. (2018) Foraminiferal growth and test development. *Earth-Sci. Rev.* **185**, 140–162.

Hohenegger J., Yordanova E., Nakano Y. and Tatzreiter F. (1999) Habitats of larger foraminifera on the upper reef slope of Sesoko Island, Okinawa, Japan. *Mar. Micropaleontol.* **36**, 109–168.

Holzmann M., Hohenegger J., Apothéloz-Perret-Gentil L., Morard R., Abramovich S., Titelboim D. and Pawlowski J. (2022) Operculina and Neoassilina: A Revision of Recent Nummulitid Genera Based on Molecular and Morphological Data Reveals a New Genus. *J. Earth Sci.* **33**, 1411–1424.

Hönisch B., Bijma J., Russell A. D., Spero H. J., Palmer M. R., Zeebe R. E. and Eisenhauer A. (2003) The influence of symbiont photosynthesis on the boron isotopic composition of foraminifera shells. *Mar. Micropaleontol.* **49**, 87–96.

Hönisch B., Hemming N. G., Archer D., Siddall M. and McManus J. F. (2009) Atmospheric Carbon Dioxide Concentration Across the Mid-Pleistocene Transition. *Science* **324**, 1551–1554.

Hottinger L. (1977) Foraminiferes Operculiniformes. PhD Thesis, Mém du Muséum Natl d'Histoire Nat.

Huang B., Liu C., Banzon V., Freeman E., Graham G., Hankins B., Smith T. and Zhang H.-M. (2021) Improvements of the Daily Optimum Interpolation Sea Surface Temperature (DOISST) Version 2.1. *J. Clim.* **34**, 2923–2939.

Humphreys M. P., Gregor L., Pierrot D., van Heuven S. M. A. C., Lewis E. R. and Wallace D. W. R. (2020) PyCO2SYS: marine carbonate system calculations in Python.

Inglis G. N., Bragg F., Burls N. J., Cramwinckel M. J., Evans D., Foster G. L., Huber M., Lunt D. J., Siler N., Steinig S., Tierney J. E., Wilkinson R., Anagnostou E., de Boer A. M., Dunkley Jones T., Edgar K. M., Hollis C. J., Hutchinson D. K. and Pancost R. D. (2020) Global mean surface temperature and climate sensitivity of the early Eocene Climatic Optimum (EECO), Paleocene–Eocene Thermal Maximum (PETM), and latest Paleocene. *Clim. Past* **16**, 1953–1968.

Jochum K. P., Garbe-Schönberg D., Veter M., Stoll B., Weis U., Weber M., Lugli F., Jentzen A., Schiebel R., Wassenburg J. A., Jacob D. E. and Haug G. H. (2019) Nano-Powdered Calcium

Carbonate Reference Materials: Significant Progress for Microanalysis? *Geostand. Geoanalytical Res.* **43**, 595–609.

Jochum K. P., Nohl U., Herwig K., Lammel E., Stoll B. and Hofmann A. W. (2005) GeoReM: A New Geochemical Database for Reference Materials and Isotopic Standards. *Geostand. Geoanalytical Res.* **29**, 333–338.

Jochum K. P., Weis U., Stoll B., Kuzmin D., Yang Q., Raczek I., Jacob D. E., Stracke A., Birbaum K., Frick D. A., Günther D. and Enzweiler J. (2011) Determination of Reference Values for NIST SRM 610-617 Glasses Following ISO Guidelines. *Geostand. Geoanalytical Res.* **35**, 397–429.

Jørgensen B. B., Erez J., Revsbech P. and Cohen Y. (1985) Symbiotic photosynthesis in a planktonic foraminiferan, Globigerinoides sacculifer (Brady), studied with microelectrodes 1. *Limnol. Oceanogr.* **30**, 1253–1267.

Jurikova H., Liebetrau V., Gutjahr M., Rollion-Bard C., Hu M. Y., Krause S., Henkel D., Hiebenthal C., Schmidt M., Laudien J. and Eisenhauer A. (2019) Boron isotope systematics of cultured brachiopods: Response to acidification, vital effects and implications for palaeo-pH reconstruction. *Geochim. Cosmochim. Acta* **248**, 370–386.

Klochko K., Cody G. D., Tossell J. A., Dera P. and Kaufman A. J. (2009) Re-evaluating boron speciation in biogenic calcite and aragonite using 11B MAS NMR. *Geochim. Cosmochim. Acta* **73**, 1890–1900.

Klochko K., Kaufman A. J., Yao W., Byrne R. H. and Tossell J. A. (2006) Experimental measurement of boron isotope fractionation in seawater. *Earth Planet. Sci. Lett.* **248**, 276–285.

Köhler-Rink S. and Kühl M. (2000) Microsensor studies of photosynthesis and respiration in larger symbiotic foraminifera. I The physico-chemical microenvironment of Marginopora vertebralis, Amphistegina lobifera and Amphisorus hemprichii. *Mar. Biol.* **137**, 473–486.

Köhler-Rink S. and Kühl M. (2005) The chemical microenvironment of the symbiotic planktonic foraminifer *Orbulina universa*. *Mar. Biol. Res.* **1**, 68–78.

ter Kuile B. and Erez J. (1987) Uptake of inorganic carbon and internal carbon cycling in symbiont-bearing benthonic foraminifera. *Mar. Biol.* **94**, 499–509.

Lauvset S. K. and Gruber N. (2014) Long-term trends in surface ocean pH in the North Atlantic. *Mar. Chem.* **162**, 71–76.

Lee K., Kim T.-W., Byrne R. H., Millero F. J., Feely R. A. and Liu Y.-M. (2010) The universal ratio of boron to chlorinity for the North Pacific and North Atlantic oceans. *Geochim. Cosmochim. Acta* **74**, 1801–1811.

Levi A., Müller W. and Erez J. (2019) Intrashell Variability of Trace Elements in Benthic Foraminifera Grown Under High CO2 Levels. *Front. Earth Sci.* **7**.

Lewis E. and Wallace D. W. R. (1998) *Program Developed for CO2 System Calculations*., Broohaven National Lab., Dept. of Applied Science, Upton, NY.

Lin L., Hu Z., Yang L., Zhang W., Liu Y., Gao S. and Hu S. (2014) Determination of boron isotope compositions of geological materials by laser ablation MC-ICP-MS using newly designed high sensitivity skimmer and sample cones. *Chem. Geol.* **386**, 22–30.

Lueker T. J., Dickson A. G. and Keeling C. D. (2000) Ocean pCO2 calculated from dissolved inorganic carbon, alkalinity, and equations for K1 and K2: validation based on laboratory measurements of CO2 in gas and seawater at equilibrium. *Mar. Chem.* **70**, 105–119.

Martínez-Botí M. A., Marino G., Foster G. L., Ziveri P., Henehan M. J., Rae J. W. B., Mortyn P. G. and Vance D. (2015) Boron isotope evidence for oceanic carbon dioxide leakage during the last deglaciation. *Nature* **518**, 219–222.

Mavromatis V., Purgstaller B., Louvat P., Faure L., Montouillout V., Gaillardet J. and Schott J. (2021) Boron isotope fractionation during the formation of amorphous calcium carbonates and their transformation to Mg-calcite and aragonite. *Geochim. Cosmochim. Acta* **315**, 152–171.

McClelland H. L. O., Halevy I., Wolf-Gladrow D. A., Evans D. and Bradley A. S. (2021) Statistical Uncertainty in Paleoclimate Proxy Reconstructions. *Geophys. Res. Lett.* **48**.

McCulloch M. T., D'Olivo J. P., Falter J., Holcomb M. and Trotter J. A. (2017) Coral calcification in a changing World and the interactive dynamics of pH and DIC upregulation. *Nat. Commun.* **8**.

Millero F. J. (2005) *Chemical oceanography*. 3rd ed., CRC press.

Müller W., Shelley M., Miller P. and Broude S. (2009) Initial performance metrics of a new custom-designed ArF excimer LA-ICPMS system coupled to a two-volume laser-ablation cell. *J Anal Spectrom* **24**, 209–214.

Nir O., Vengosh A., Harkness J. S., Dwyer G. S. and Lahav O. (2015) Direct measurement of the boron isotope fractionation factor: Reducing the uncertainty in reconstructing ocean paleo-pH. *Earth Planet. Sci. Lett.* **414**, 1–5.

Oron S., Abramovich S., Almogi-Labin A., Woeger J. and Erez J. (2018) Depth related adaptations in symbiont bearing benthic foraminifera: New insights from a field experiment on Operculina ammonoides. *Sci. Rep.* **8**.

Oron S., Evans D., Abramovich S., Almogi-Labin A. and Erez J. (2020) Differential Sensitivity of a Symbiont-Bearing Foraminifer to Seawater Carbonate Chemistry in a Decoupled DIC-pH Experiment. *J. Geophys. Res. Biogeosciences* **125**.

Orr J. C., Epitalon J.-M., Dickson A. G. and Gattuso J.-P. (2018) Routine uncertainty propagation for the marine carbon dioxide system. *Mar. Chem.* **207**, 84–107.

Özcan E., Less Gy., Jovane L., Catanzariti R., Frontalini F., Coccioni R., Giorgioni M., Rodelli D., Rego E. S., Kayğılı S. and Asgharian Rostami M. (2019) Integrated biostratigraphy of the middle to upper Eocene Kırkgeçit Formation (Baskil section, Elazığ, eastern Turkey): larger benthic foraminiferal perspective. *Mediterr. Geosci. Rev.* **1**, 55–90.

PALAEOSENS (2012) Making sense of palaeoclimate sensitivity. *Nature* **491**, 683–691.

Parkhurst D. L. and Appelo C. A. J. (2013) Description of input and examples for PHREEQC version 3: a computer program for speciation, batch-reaction, one-dimensional transport, and inverse geochemical calculations.

Pokrovski G. S., Schott J. and Sergeyev A. S. (1995) Experimental determination of the stability constants of NaSO4− and NaB (OH)40 in hydrothermal solutions using a new high-temperature sodium-selective glass electrode — Implications for boron isotopic fractionation. *Chem. Geol.* **124**, 253–265.

Poloczanska E., Mintenbeck K., Portner H. O., Roberts D. and Levin L. A. (2018) The IPCC special report on the ocean and cryosphere in a changing climate. In *2018 Ocean Sciences Meeting* AGU.

Rae J. W. B. (2018) Boron Isotopes in Foraminifera: Systematics, Biomineralisation, and CO2 Reconstruction. In *Boron Isotopes* Advances in Isotope Geochemistry. Springer. pp. 107–143.

Rae J. W. B., Foster G. L., Schmidt D. N. and Elliott T. (2011) Boron isotopes and B/Ca in benthic foraminifera: Proxies for the deep ocean carbonate system. *Earth Planet. Sci. Lett.* **302**, 403–413.

Raimondi L., Matthews J. B. R., Atamanchuk D., Azetsu-Scott K. and Wallace D. W. R. (2019) The internal consistency of the marine carbon dioxide system for high latitude shipboard and in situ monitoring. *Mar. Chem.* **213**, 49–70.

Renema W. (2008) Habitat selective factors influencing the distribution of larger benthic foraminiferal assemblages over the Kepulauan Seribu. *Mar. Micropaleontol.* **68**, 286–298.

Renema W. (2002) Larger foraminfera as marine environmental indicators. *Scr. Geol.* **124**, 1–260.

Renema W., Beaman R. J. and Webster J. M. (2013) Mixing of relict and modern tests of larger benthic foraminifera on the Great Barrier Reef shelf margin. *Mar. Micropaleontol.* **101**, 68–75.

Renema W. and Troelstra S. R. (2001) Larger foraminifera distribution on a mesotrophic carbonate shelf in SW Sulawesi (Indonesia). *Palaeogeogr. Palaeoclimatol. Palaeoecol.* **175**, 125–146.

Rink S., Kühl M., Bijma J. and Spero H. J. (1998) Microsensor studies of photosynthesis and respiration in the symbiotic foraminifer Orbulina universa. *Mar. Biol.* **131**, 583–595.

Rollion-Bard C. and Erez J. (2010) Intra-shell boron isotope ratios in the symbiont-bearing benthic foraminiferan Amphistegina lobifera: Implications for $\updelta$11B vital effects and paleo-pH reconstructions. *Geochim. Cosmochim. Acta* **74**, 1530–1536.

Rosman K. J. R. and Taylor P. D. P. (1997) Isotopic composition of the elements 1997.

Sadekov A., Lloyd N. S., Misra S., Trotter J., D’Olivo J. and McCulloch M. (2019) Accurate and precise microscale measurements of boron isotope ratios in calcium carbonates using laser ablation multicollector-ICPMS. *J. Anal. At. Spectrom.* **34**, 550–560.

Sanyal A., Bijma J., Spero H. and Lea D. W. (2001) Empirical relationship between pH and the boron isotopic composition of *Globigerinoides sacculifer* : Implications for the boron isotope paleo-pH proxy. *Paleoceanography* **16**, 515–519.

Sanyal A., Hemming N. G., Broecker W. S., Lea D. W., Spero H. J. and Hanson G. N. (1996) Oceanic pH control on the boron isotopic composition of foraminifera: Evidence from culture experiments. *Paleoceanography* **11**, 513–517.

Sanyal A., Hemming N. G., Hanson G. N. and Broecker W. S. (1995) Evidence for a higher pH in the glacial ocean from boron isotopes in foraminifera. *Nature* **373**, 234–236.

Segev E. and Erez J. (2006) Effect of Mg/Ca ratio in seawater on shell composition in shallow benthic foraminifera. *Geochem. Geophys. Geosystems* **7**.

Standish C. D., Chalk T. B., Babila T. L., Milton J. A., Palmer M. R. and Foster G. L. (2019) The effect of matrix interferences on in situ boron isotope analysis by laser ablation multi-collector inductively coupled plasma mass spectrometry. *Rapid Commun. Mass Spectrom.* **33**, 959–968.

Stewart J. A., Christopher S. J., Kucklick J. R., Bordier L., Chalk T. B., Dapoigny A., Douville E., Foster G. L., Gray W. R., Greenop R., Gutjahr M., Hemsing F., Henehan M. J., Holdship P., Hsieh Y., Kolevica A., Lin Y., Mawbey E. M., Rae J. W. B., Robinson L. F., Shuttleworth R., You C., Zhang S. and Day R. D. (2021) NIST RM 8301 Boron Isotopes in Marine Carbonate (Simulated Coral and Foraminifera Solutions): Inter-laboratory δ^{11}B and Trace Element Ratio Value Assignment. *Geostand. Geoanalytical Res.* **45**, 77–96.

Tierney J. E., Zhu J., King J., Malevich S. B., Hakim G. J. and Poulsen C. J. (2020) Glacial cooling and climate sensitivity revisited. *Nature* **584**, 569–573.

Toyofuku T., Matsuo M. Y., de Nooijer L. J., Nagai Y., Kawada S., Fujita K., Reichart G.-J., Nomaki H., Tsuchiya M., Sakaguchi H. and Kitazato H. (2017) Proton pumping accompanies calcification in foraminifera. *Nat. Commun.* **8**, 14145.

Trotter J., Montagna P., McCulloch M., Silenzi S., Reynaud S., Mortimer G., Martin S., Ferrier-Pagès C., Gattuso J.-P. and Rodolfo-Metalpa R. (2011) Quantifying the pH `vital effect' in the temperate zooxanthellate coral Cladocora caespitosa: Validation of the boron seawater pH proxy. *Earth Planet. Sci. Lett.* **303**, 163–173.

Van Dijk I., De Nooijer L. J. and Reichart G.-J. (2017) Trends in element incorporation in hyaline and porcelaneous foraminifera as a function of pCO2. *Biogeosciences* **14**, 497–510.

Virtanen P., Gommers R., Oliphant T. E., Haberland M., Reddy T., Cournapeau D., Burovski E., Peterson P., Weckesser W., Bright J., van der Walt S. J., Brett M., Wilson J., Millman K. J., Mayorov N., Nelson A. R. J., Jones E., Kern R., Larson E., Carey C. J., Polat İ., Feng Y., Moore E. W., VanderPlas J., Laxalde D., Perktold J., Cimrman R., Henriksen I., Quintero E. A., Harris C. R., Archibald A. M., Ribeiro A. H., Pedregosa F., van Mulbregt P., and SciPy 1.0 Contributors (2020) SciPy 1.0: Fundamental Algorithms for Scientific Computing in Python. *Nat. Methods* **17**, 261–272.

Westerhold T., Marwan N., Drury A. J., Liebrand D., Agnini C., Anagnostou E., Barnet J. S. K., Bohaty S. M., Vleeschouwer D. D., Florindo F., Frederichs T., Hodell D. A., Holbourn A. E., Kroon D., Lauretano V., Littler K., Lourens L. J., Lyle M., Pälike H., Röhl U., Tian J., Wilkens R. H., Wilson P. A. and Zachos J. C. (2020) An astronomically dated record of Earth's climate and its predictability over the last 66 million years. *Science* **369**, 1383–1387.

Williams N. L., Juranek L. W., Feely R. A., Johnson K. S., Sarmiento J. L., Talley L. D., Dickson A. G., Gray A. R., Wanninkhof R., Russell J. L., Riser S. C. and Takeshita Y. (2017) Calculating surface ocean pCO_2 from biogeochemical Argo floats equipped with pH: An uncertainty analysis: Calculating Ocean pCO_2 From Float pH. *Glob. Biogeochem. Cycles* **31**, 591–604.

Wolf-Gladrow D. A., Bijma J. and Zeebe R. E. (1999) Model simulation of the carbonate chemistry in the microenvironment of symbiont bearing foraminifera. *Mar. Chem.* **64**, 181–198.

Yu J. and Elderfield H. (2007) Benthic foraminiferal B/Ca ratios reflect deep water carbonate saturation state. *Earth Planet. Sci. Lett.* **258**, 73–86.

Yu J., Elderfield H. and Hönisch B. (2007) B/Ca in planktonic foraminifera as a proxy for surface seawater pH. *Paleoceanography* **22**.

Zachos J., Pagani M., Sloan L., Thomas E. and Billups K. (2001) Trends, rhythms, and aberrations in global climate 65 Ma to present. *Science* **292**, 686–693.

Zeebe R. E. and Rae J. W. B. (2020) Equilibria, kinetics, and boron isotope partitioning in the aqueous boric acid–hydrofluoric acid system. *Chem. Geol.* **550**, 119693.

Zeebe R. E. and Tyrrell T. (2019) History of carbonate ion concentration over the last 100 million years II: Revised calculations and new data. *Geochim. Cosmochim. Acta* **257**, 373–392.

Zeebe R. E. and Wolf-Gladrow D. (2001) *CO2 in seawater: equilibrium, kinetics, isotopes*., Gulf Professional Publishing.

Zeebe R. E., Wolf-Gladrow D. A., Bijma J. and Hönisch B. (2003) Vital effects in foraminifera do not compromise the use of d11B as a paleo-pH indicator: Evidence from modeling. *Paleoceanography* **18**.

Table 1: Measured and calculated chemistry of the culture baths for *Operculina ammonoides*. The bath pH and alkalinity were both measured, but the weighted pH bad alkalinity were calculated (see text). Carbonate parameters were calculated using pyCO2SYS and the weighted pH and alkalinity were used as inputs. The reported uncertainty for the saturation state of calcite ($\Omega_{calcite}$) are the median (50th percentile) and lower/upper percentiles corresponding to 2SD. This was reported instead of a normal 2SD because the resulting MC dataset is not normally distributed (see text).

Sample	Bath pH (NBS) Mean	Bath pH (NBS) 2 SD	Bath Alk (µEq/L) Mean	Bath Alk (µEq/L) 2 SD	pH_W (NBS) Mean	pH_W (NBS) 2 SE	Alk_W (µEq/L) Mean	Alk_W (µEq/L) 2 SE	DIC (µmol/L) Mean	DIC (µmol/L) 2 SD	$\Omega_{calcite}$ 2.5th	$\Omega_{calcite}$ 50th	$\Omega_{calcite}$ 97.5th
HH6-1	7.43	0.26	2205	21	7.49	0.15	1988	93	1964	104	0.83	1.14	1.56
HH6-2	7.66	0.19	2350	7	7.6	0.15	2034	118	1971	127	1.08	1.5	2.07
HH6-3	8.03	0.08	2495	14	7.89	0.24	2077	128	1903	160	1.70	2.75	4.29
HH6-4	8.37	0.31	2929	10	8.33	0.12	2333	172	1886	172	5.48	6.71	8.09
HH6-5	7.85	0.39	2507	22	7.74	0.16	2046	149	1937	156	1.68	2.34	3.22
HH6-6	7.51	0.38	2348	8	7.54	0.04	2006	165	1962	165	1.75	1.98	2.24
HH7-1	7.99	0.15	2832	12	7.95	0.12	2536	102	2334	115	2.76	3.51	4.42
HH7-2	7.73	0.61	938	50	7.91	0.07	832	27	731	26	0.98	1.02	1.07
HH7-3	7.84	0.38	1276	13	7.83	0.08	1130	41	1037	46	1.02	1.2	1.4
HH7-4	7.77	0.53	1580	408	7.77	0.03	1422	58	1334	57	1.27	1.37	1.48
HH7-5	7.99	0.34	2348	22	7.96	0.09	2084	78	1903	83	2.46	2.92	3.43
HH7-6	8.09	0.11	2264	5	7.93	0.18	2016	154	1850	164	1.84	2.65	3.74

Table 2: Resulting measured boron isotopic composition of cultured *Operculina ammonoides*. $\delta^{11}B_{B(OH)4-}$ was calculated using a Monte Carlo approach and used the weighted carbonate parameters as inputs (see text). The uncertainty of $\delta^{11}B_{B(OH)4-}$ is reported as percentiles of the 10^5 Monte Carlo simulated values.

Sample	pH_W (Total) Mean	pH_W (NBS) 2 SE	$\delta^{11}B_{B(OH)4-}$ (‰) 50^{th}	$\delta^{11}B_{B(OH)4-}$ (‰) 2.5^{th}	$\delta^{11}B_{B(OH)4-}$ (‰) 97.5^{th}	$\delta^{11}B_{CaCO3}$ (‰) Mean	$\delta^{11}B_{CaCO3}$ (‰) 2 SE	B/Ca (mmol/mol) Mean	B/Ca (mmol/mol) 2 SE
HH6-1	7.35	0.15	13.63	13.19	14.2	16.09	0.62	0.21	0.03
HH6-2	7.47	0.15	14.08	13.51	14.85	16.86	0.38	0.26	0.02
HH6-3	7.76	0.24	15.73	14.32	17.85	17.56	0.48	0.36	0.03
HH6-4	8.2	0.12	20.22	18.8	21.8	19.45	0.34	0.45	0.03
HH6-5	7.61	0.16	14.77	14	15.8	17.71	0.23	0.33	0.02
HH6-6	7.41	0.04	13.89	13.72	14.07	17.41	0.41	0.31	0.03
HH7-1	7.81	0.12	15.98	15.14	16.99	17.55	0.25	0.28	0.02
HH7-2	7.78	0.01	15.73	15.63	15.82	18.07	0.26	0.36	0.02
HH7-3	7.69	0.08	15.14	14.68	15.67	17.75	0.21	0.31	0.02
HH7-4	7.64	0.03	14.81	14.64	14.99	17.32	0.24	0.28	0.02
HH7-5	7.82	0.08	16.05	15.43	16.75	17.19	0.27	0.28	0.01
HH7-6	7.79	0.18	15.81	14.67	17.36	17.85	0.38	0.32	0.02

Table 3: Details of the field collected *Operculina ammonoides*. Alkalinity (TAlk), pH and temperature (T) were taken from global dataset (see text). $\delta^{11}B_{B(OH)4-}$ was calculated from the aforementioned parameters using a Monte Carlo approach (see text). GBR stands for Great Barrier Reef.

Sample	Location	Lat (decimal degrees)	Long (decimal degrees)	pH (total) mean	pH (total) 2 SD	TAlk (µmol/kg) Mean	TAlk (umol/kg) 2 SD	T (°C) Mean	T (°C) 2 SD	$\delta^{11}B_{B(OH)4-}$ (‰) 50th	$\delta^{11}B_{B(OH)4-}$ (‰) 2.5th	$\delta^{11}B_{B(OH)4-}$ (‰) 97.5th	$\delta^{11}B_{CaCO3}$ (‰) Mean	$\delta^{11}B_{CaCO3}$ (‰) 2 SE	B/Ca (mmol/mol) Mean	B/Ca (mmol/mol) 2 SE
PD28	Makassar	5.06	119.42	8.08	0.01	2208	45	29	1.2	19.09	18.79	19.39	18.01	0.28	0.25	0.02
SSO7G14	GBR	-19.73	115.22	8.09	0.03	2303	32	26.6‡	3.5‡	18.84	18.07	19.62	18.55	0.2	0.39	0.02
SER	Jakarta	-5.51	106.56	8.06	0.03	2166	46	29‡	0.5‡	18.73	18.41	19.04	16.09	0.32	0.39	0.02
Eil19	Gulf of Eilat	29.54	34.97	7.99	0.05	2486	69	21.9‡	0.8‡	17.19	16.69	17.72	18.00	0.28	0.32	0.02
BBX49a	Celebes Sea	1.39	118.82	7.9†	0.02†	2213	53	29.2‡	0.9‡	17.19	16.98	17.4	17.05	0.41	0.33	0.03
KKE30	Makassar	-5.11	119.29	7.86†	0.12†	2205	66	28‡	0.4‡	16.65	15.73	17.75	16.84	0.22	0.27	0.01

† pH measurement from nearby reefs
‡ Temperature taken from Evans et al. (2013).

Evans, D., Brierley, C., Raymo, M.E., Erez, J. and Müller, W. (2016) Planktic foraminifera shell chemistry response to seawater chemistry: Pliocene–Pleistocene seawater Mg/Ca, temperature and sea level change. Earth Planet. Sci. Lett. 438, 139-148.
Müller, W., Shelley, M., Miller, P. and Broude, S. (2009) Initial performance metrics of a new custom-designed ArF excimer LA-ICPMS system coupled to a two-volume laser-ablation cell. Journal Analytical Atomic Spectrometry 24, 209-214.